nature communications

Article

https://doi.org/10.1038/s41467-025-59184-5

ZMYND8 drives HER2 antibody resistance in breast cancer via lipid control of IL-27

Received: 7 June 2024

Accepted: 11 April 2025

Published online: 25 April 2025

Check for updates

Yong Wang[1], Yanan Wang[1], Lei Bao[1], Goncalo Vale[2,3], Jeffrey G. McDonald[2,3], Yisheng Fang[1], Yan Peng[1], Ashwani Kumar[4], Chao Xing[4,5], Fara Brasó-Maristany[6,7,8], Aleix Prat[6,7,8,9,10], Carlos L. Arteaga[11], Yingfei Wang[1,11,12,13] & Weibo Luo[1,11,14]

Anti-HER2 antibodies are effective but often lead to resistance in patients with HER2+ breast cancer. Here, we report an epigenetic crosstalk with aberrant glycerophospholipid metabolism and inflammation as a key resistance mechanism of anti-HER2 therapies in HER2+ breast cancer. Histone reader ZMYND8 specifically confers resistance to cancer cells against trastuzumab and/or pertuzumab. Mechanistically, ZMYND8 enhances cPLA2α expression in resistant tumor cells through inducing c-Myc. cPLA2α inactivates phosphatidylcholine-specific phospholipase C to inhibit phosphatidylcholine breakdown into diacylglycerol, which diminishes protein kinase C activity leading to interleukin-27 secretion. Supplementation with interleukin-27 protein counteracts cPLA2α loss to reinforce trastuzumab resistance in HER2+ tumor cells and patient-derived organoids. Upregulation of ZMYND8, c-Myc, cPLA2α, and IL-27 is prevalent in HER2+ breast cancer patients following HER2-targeted therapies. Targeting c-Myc or cPLA2α effectively overcomes anti-HER2 therapy resistance in patient-derived xenografts. Collectively, this study uncovers a druggable signaling cascade that drives resistance to HER2-targeted therapies in HER2+ breast cancer.

Human epidermal growth factor receptor 2-positive (HER2+) breast cancer, accounting for ~15% of all breast cancer cases, is an aggressive subtype whose growth is reliant on overexpression (OE) of the HER2 receptor tyrosine kinase. The current standard of care for HER2+ breast cancer involves targeting HER2 with anti-HER2 monoclonal antibodies and/or tyrosine kinase inhibitors, which has remarkably improved outcomes for patients with early disease[1,2]. The FDA-approved antibodies, including trastuzumab, pertuzumab, and ado-trastuzumab emtansine (T-DM1), bind HER2 protein on the surface of cancer cells to block HER2-mediated signaling pathways that control cancer cell proliferation or elicit cytotoxic effects in cancer cells[3]. Large clinical studies have demonstrated that the dual HER2 blockade with trastuzumab plus pertuzumab achieves a higher pathological complete response rate than either drug alone in the neoadjuvant setting and thus it is FDA approved as first-line therapy in combination with chemotherapy for patients with early and advanced HER2+ breast

[1]Department of Pathology, UT Southwestern Medical Center, Dallas, TX, USA. [2]Center for Human Nutrition, UT Southwestern Medical Center, Dallas, TX, USA. [3]Department of Molecular Genetics, UT Southwestern Medical Center, Dallas, TX, USA. [4]Eugene McDermott Center for Human Growth and Development, UT Southwestern Medical Center, Dallas, TX, USA. [5]Lyda Hill Department of Bioinformatics, UT Southwestern Medical Center, Dallas, TX, USA. [6]Translational Genomics and Targeted Therapies in Solid Tumors, August Pi i Sunyer Biomedical Research Institute (IDIBAPS), Barcelona, Spain. [7]Cancer Institute and Blood Diseases, Hospital Clínic of Barcelona, Barcelona, Spain. [8]Reveal Genomics, S.L., Barcelona, Spain. [9]University of Barcelona, Barcelona, Spain. [10]Institute of Oncology-Hospital Quirónsalud, Barcelona, Spain. [11]Harold C. Simmons Comprehensive Cancer Center, UT Southwestern Medical Center, Dallas, TX, USA. [12]Department of Neurology, UT Southwestern Medical Center, Dallas, TX, USA. [13]Peter O'Donnell Jr. Brain Institute, UT Southwestern Medical Center, Dallas, TX, USA. [14]Department of Pharmacology, UT Southwestern Medical Center, Dallas, TX, USA. e-mail: Weibo.Luo@UTSouthwestern.edu

cancer[4–6]. Despite the initial response to HER2-targeted therapies, many patients with metastatic HER2+ breast cancer often have therapy resistance and experience tumor recurrence, ultimately leading to death of the disease[7]. Previous studies have identified several trastuzumab resistance mechanisms, including genetic alterations in *ERBB2* gene (encoding HER2 protein), hyperactivation of phosphoinositide 3-kinase (PI3K) signaling and alternate signaling pathways, and immune evasion[3,7]. However, these alterations may not explain all de novo and acquired mechanisms of drug resistance to the double HER2 blockade with trastuzumab and pertuzumab. While HER2-targeted antibody drug conjugates, like trastuzumab deruxtecan (T-DXd) and T-DM1, are effective in patients, there are some limitations associated with their use, including therapy resistance, toxicities, limited impact on heterogeneous tumors, and high costs. Thus, understanding the mechanism of resistance to trastuzumab plus pertuzumab is crucial, because it will not only provide insights into diverse adaptive mechanisms and biomarkers, but also contribute to optimizing combination therapies and to the development of personalized therapies capable of preventing treatment resistance and inducing cures.

Epigenetic alterations are often induced by cancer treatments and drive the therapy resistance. The histone reader ZMYND8 is a member of bromodomain family proteins and acts as an oncoprotein to promote growth of human cancers, including brain, colorectal, kidney, liver, and estrogen-positive/triple-negative breast cancers[8–12]. It interacts with transcription factors and epigenetic modifiers to modulate the expression of genes whose protein products contribute to angiogenesis, antioxidant response, cell migration and invasion, DNA damage response, epithelial-mesenchymal transition, innate immune response, and metabolism in cancer cells[8,13–17]. A recent bioinformatics analysis reported that, amongst bromodomain family members, only ZMYND8 mRNA was upregulated in human HER2+ breast tumors resistant to trastuzumab[18]. However, the role of ZMYND8 in anti-HER2 therapy resistance remains unknown.

Metabolic reprogramming is another hallmark of human cancers and frequently induced by oncogenes such as c-Myc[19]. HER2+ breast cancer cells have the elevated levels of glycerophospholipids including phosphatidylcholine (PC), phosphatidylethanolamine (PE), and triacylglycerol (TAG), compared with other subtypes of breast cancer cells[20]. PC is the most abundant glycerophospholipid that acts as a major structural component of cell membrane in eukaryotes. It is synthetized via the de novo Kennedy pathway and the remodeling pathway (Lands' cycle) and broken down by a family of phospholipases leading to generation of the second messengers involved in inflammation, cell death, and immunity[21]. Cytosolic phospholipase A2 alpha (cPLA2α) is a well-characterized phospholipase isoform and activated by intracellular calcium and kinases[22]. cPLA2α preferentially catalyzes the hydrolysis of the sn-2 ester bond of glycerophospholipids to produce arachidonic acid (AA) and lysophospholipids[22]. Previous studies have shown upregulation of cPLA2α promoting breast cancer metastasis[23], however, its precise mechanism remains largely unknown. Whether cPLA2α associates with elevated glycerophospholipids contributing to HER2-targeted therapy resistance has not been explored yet.

Here, we show that ZMYND8 is more potently induced in HER2+ human breast cancers resistant to anti-HER2 therapies. ZMYND8 is necessary and sufficient to drive trastuzumab or trastuzumab plus pertuzumab resistance in preclinical models of HER2+ breast cancer. ZMYND8 activates the c-Myc-cPLA2α axis to inhibit PC metabolic breakdown into diacylglycerol (DAG) in tumor cells, which causes inactivation of protein kinase C (PKC) to induce interleukin-27 (IL-27) expression, thereby mediating tumor resistance to the HER2 antibodies. Genetic or pharmacological inhibition of c-Myc or cPLA2α markedly re-sensitizes patient-derived xenografts (PDXs) and tumor organoids to trastuzumab or trastuzumab plus pertuzumab in vitro and in mice. Collectively, these findings define the ZMYND8-c-Myc-cPLA2α-IL-27 axis as the molecular mechanism of anti-HER2 therapy resistance and identify both c-Myc and cPLA2α as druggable targets capable of surmounting HER2+ breast tumor resistance to HER2-targeted therapies.

Results

ZMYND8 protein is upregulated in human HER2+ breast cancer resistant to HER2 antibodies plus chemotherapy

To investigate the role of ZMYND8 in HER2+ breast cancer, we queried *ZMYND8* mRNA in The Cancer Genome Atlas (TCGA) cohort and found increased *ZMYND8* mRNA levels in HER2+ breast tumors compared with normal breast tissues (Supplementary Fig. 1a). To assess ZMYND8 upregulation at the protein level, we performed immunohistochemistry (IHC) with anti-ZMYND8 antibody in human HER2+ tumors. ZMYND8 protein levels were significantly elevated in tumor cells (Supplementary Fig. 1b, c). Notably, breast cancer patients with lower tumoral ZMYND8 expression achieved a complete response to HER2 antibodies-based therapies, whereas those with higher expression had only a partial or no response (Fig. 1a and Supplementary Table 1). We further analyzed HER2+ breast tumors harvested from the same patients before and after HER2-targeted therapy, and found ZMYND8 protein upregulation in tumors resistant to trastuzumab, pertuzumab, and docetaxel (Fig. 1b, c). In line with human tumors, ZMYND8 protein was upregulated in trastuzumab-resistant HR6 cells as compared with isogenic trastuzumab-responsive BT474T cells (Fig. 1d and Supplementary Fig. 1d, e), both of which were isolated from HER2 overexpressing BT474 xenografts in mice treated with or without trastuzumab, respectively[24]. Intriguingly, *ZMYND8* mRNA was not induced in human HER2+ breast tumors after neoadjuvant treatment with trastuzumab plus lapatinib in the PAMELA clinical trial[25] (Supplementary Fig. 1f). Similar results were found in pre-treated HER2+ breast tumors from patients with pathologic complete response *vs*. those with residual disease as well as in BT474T *vs*. HR6 cells (Supplementary Fig. 1g, h). These results suggest that ZMYND8 is upregulated by HER2 targeted therapies at the protein level. To determine the specificity of ZMYND8 induction in HER2 antibody-resistant tumor cells, we studied ZMYND8 expression in two neratinib-resistant cell lines, OVCAR8NR and 5637NR, and found no changes in ZMYND8 protein levels between resistant cells and their isogenic counterparts (Supplementary Fig. 1i). Similarly, the chemotherapy drug, docetaxel, failed to induce ZMYND8 expression in BT474T cells (Supplementary Fig. 1j). Kaplan–Meier survival analysis showed that ZMYND8 negatively correlated with overall survival of patients with HER2+ breast cancer (Supplementary Fig. 1k). Collectively, these results indicate that ZMYND8 is induced in human HER2+ breast cancer by the current standard of care with anti-HER2 antibodies plus chemotherapy, which may predict a poorer therapeutic response.

ZMYND8 induction confers HER2 antibody resistance in HER2+ breast cancer

To determine whether ZMYND8 regulates HER2+ breast cancer progression, we deleted *ZMYND8* in SK-BR-3 cells using CRISPR/Cas9, and found that knockout (KO) of ZMYND8 significantly inhibited colony growth and migration of SK-BR-3 cells (Supplementary Fig. 2a–e). Next, we took advantages of isogenic HR6 and BT474T cells to study whether ZMYND8 drives trastuzumab resistance in HER2+ breast cancer. ZMYND8 KO significantly reduced HR6 colony growth without affecting HER2 expression (Fig. 1e and Supplementary Fig. 2f, g). Next, we seeded ZMYND8 KO1 or KO2 HR6 cells 1.5-fold more than HR6 cells to achieve their comparable colony numbers among vehicle groups in clonogenic survival studies. Trastuzumab killed ZMYND8 KO1 or KO2 cells but not parental HR6 cells in a dose-dependent manner (Fig. 1f, g). Sensitization of HR6 cells to 0.25 μg/mL trastuzumab was also observed when ZMYND8 protein was knocked down with either of two

https://doi.org/10.1038/s41467-025-59184-5

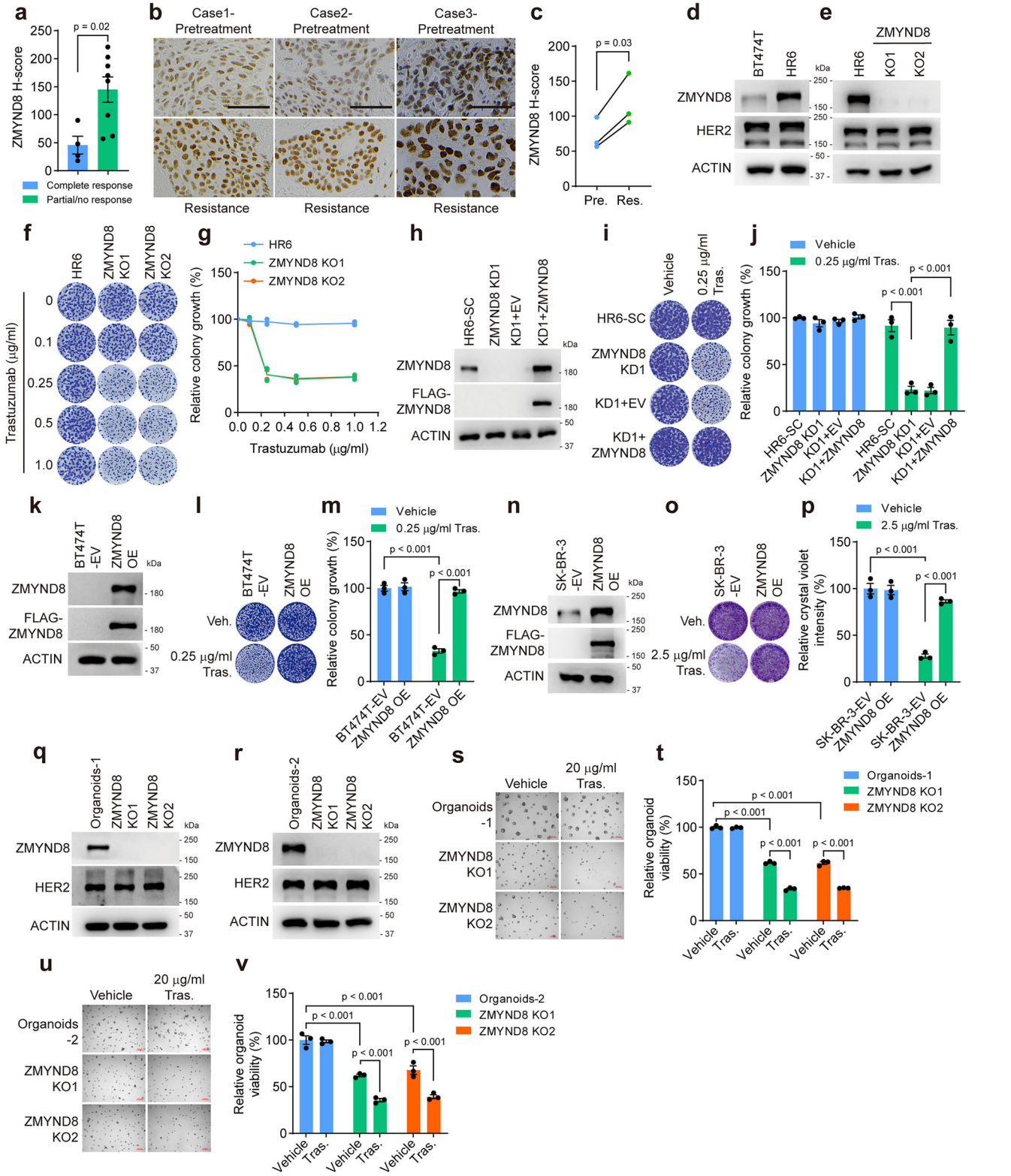

independent short hairpin RNAs (shRNAs), which was counteracted by re-expression of ZMYND8 (Fig. 1h-j and Supplementary Fig. 2h–j), suggesting a specific role of ZMYND8 in trastuzumab resistance. Contrary to ZMYND8 loss-of-function, ZMYND8 OE rendered both BT474T and SK-BR-3 cells resistant to trastuzumab treatment (Fig. 1k–p and Supplementary Fig. 2k, l). To validate the role of ZMYND8 in trastuzumab resistance observed in isogenic cell lines, we generated three-dimensional organoids from two HER2 therapy-resistant breast cancer PDX characterized by strong ZMYND8 expression (Fig. 1q, r). The organoids maintained HER2 antibody-resistant properties (Fig. 1s–v). ZMYND8 was depleted by its single guide RNAs (sgRNAs) without altering HER2 protein levels (Fig. 1q, r). ZMYND8 KO1 or KO2 significantly suppressed organoid growth and further reduced organoid viability following 20 μg/mL trastuzumab treatment, indicating that ZMYND8 promotes trastuzumab resistance in HER2+ tumor organoids (Fig. 1s–v).

Fig. 1 | ZMYND8 drives trastuzumab resistance in HER2+ breast cancer in vitro. **a** ZMYND8 IHC analysis in human HER2+ breast tumors with complete ($n = 4$) or partial/no response ($n = 8$) to HER2-targeted therapy. **b**, **c** ZMYND8 IHC analysis in human HER2+ breast tumors before and after trastuzumab+pertuzumab+docetaxel treatment. Representative IHC images (**b**) and quantification (**c**, $n = 3$). **d** Immunoblot analysis of ZMYND8 and HER2 proteins in BT474T and HR6 cells ($n = 3$). **e** Immunoblot analysis of ZMYND8 and HER2 proteins in parental and ZMYND8 KO HR6 cells ($n = 3$). **f**, **g** Clonogenic growth of parental and ZMYND8 KO HR6 cells treated with vehicle or trastuzumab for 6 days. Representative colony images (**f**) and quantification (**g**, $n = 2$). **h** Immunoblot analysis of ZMYND8 protein in SC, ZMYND8 KD1, and ZMYND8-rescued HR6 cells ($n = 3$). **i**, **j** Clonogenic growth of SC, ZMYND8 KD1, KD1 + EV, and KD1 + ZMYND8 HR6 cells treated with vehicle or trastuzumab (Tras.) for 6 days. Representative colony images (**i**) and quantification (**j**, $n = 3$). **k** Immunoblot analysis of ZMYND8 protein in EV- and ZMYND8-BT474T cells ($n = 3$). **l**, **m** Clonogenic growth of EV- and ZMYND8-BT474T cells treated with vehicle or trastuzumab for 6 days. Representative colony images (**l**) and quantification (**m**, $n = 3$). **n** Immunoblot analysis of ZMYND8 protein in EV- and ZMYND8-SK-BR-3 cells ($n = 3$). **o**, **p** Clonogenic growth of EV- and ZMYND8-SK-BR-3 cells treated with vehicle or trastuzumab for 6 days. Representative colony images (**o**) and quantification (**p**, $n = 3$). **q**, **r** Immunoblot analysis of ZMYND8 and HER2 proteins in parental and ZMYND8 KO organoids ($n = 2$). **s**–**v** Growth of parental, ZMYND8 KO1 and KO2 organoids-1 treated with vehicle or trastuzumab for 9 days. Representative organoid images (**s**, **u**) and organoid viability quantification (**t**, **v**, $n = 3$). Data from biological replicates represent mean ± SEM. *P*-value was determined by two-way ANOVA with Tukey's test (**j**, **m**, **p**, **t**, and **v**), unpaired 2-tailed Student's *t*-test (**a**), or paired 2-tailed Student's *t*-test (**c**). Scale bar, 50 μm (**b**) or 200 μm (**s**, **u**). Source data are provided as a Source Data file.

To determine the specificity of ZMYND8 in trastuzumab resistance, we treated BT474T cells overexpressing ZMYND8 or empty vector (EV) with the HER2 tyrosine inhibitor lapatinib or neratinib and found that ZMYND8 OE did not affect the response of BT474T cells to lapatinib or neratinib (Supplementary Fig. 3a–d). Similarly, ZMYND8 KO1 or KO2 did not alter the sensitivity of BT474T cells, SK-BR-3 cells, and organoids to lapatinib, neratinib, or docetaxel (Supplementary Fig. 4a–r), although ZMYND8 KO significantly inhibited the growth of BT474T and SK-BR-3 cells (Supplementary Fig. 5a–f). Together, these findings uncover a specific role of ZMYND8 in driving trastuzumab resistance in HER2+ breast cancer.

HR6 cells were also resistant to 20-50 μg/mL pertuzumab alone or 0.2 μg/mL (lower dose) trastuzumab plus 20–50 μg/mL pertuzumab (Fig. 2a, b). ZMYND8 KO1 or KO2 re-sensitized HR6 cells to 0.2 μg/mL trastuzumab plus 50 μg/mL pertuzumab (Fig. 2a, b), whereas ZMYND8 OE significantly increased BT474T cell resistance to 0.25 μg/mL trastuzumab plus 50 μg/mL pertuzumab (Fig. 2c, d). Likewise, tumor organoid resistance to 2 μg/mL (lower dose) trastuzumab plus 50 μg/mL pertuzumab was also alleviated by ZMYND8 KO1 or KO2 (Fig. 2e–h). Collectively, our data indicate that ZMYND8 is necessary and sufficient to drive resistance to trastuzumab or trastuzumab plus pertuzumab in HER2+ breast cancer cells and organoids.

To determine if ZMYND8 drives trastuzumab resistance in HER2+ breast tumors in vivo, we implanted HR6 and ZMYND8 KO1 or KO2 cells into the mammary fat pad of female NSG mice, respectively. Mice were administrated intraperitoneally with vehicle or 20 mg/kg trastuzumab twice per week for 2 weeks when the tumor volume reached ~100 mm^3. ZMYND8 KO1 or KO2 effectively inhibited HR6 tumor growth (Fig. 3a, b). Trastuzumab treatment, though unable to block HR6 tumor growth, synergized with ZMYND8 KO1 or KO2 to induce tumor regression in mice (Fig. 3a, b). In contrast, ZMYND8 OE significantly reduced sensitivity of BT474T tumors to trastuzumab at both high (15 mg/kg) and low (5 mg/kg) doses in mice (Fig. 3c–e). Taken together, our results indicate that ZMYND8 drives trastuzumab resistance in HER2+ breast tumors in vivo.

c-Myc induction by ZMYND8 is responsible for HER2 antibody resistance in HER2+ breast cancer

To determine whether ZMYND8 downstream target genes mediate HER2 antibody resistance, we analyzed ZMYND8 transcriptome in isogenic BT474T and HR6 cells by RNA-sequencing (RNA-seq). 2066 genes were differentially regulated in HR6 cells compared with BT474T cells (Supplementary Fig. 6a). However, ZMYND8 KO inhibited 176 genes but induced 400 genes in HR6 cells (FDR < 0.05, LogCPM > 0, |fold change| > 2, Supplementary Fig. 6a). Hallmark pathway analysis with gene set enrichment analysis (FDR < 0.1) revealed, amongst differentially expressed genes, only c-Myc target genes were inhibited by both ZMYND8 KO1 and KO2, although a couple of signaling pathways were enriched in HR6 cells (Supplementary Fig. 6b–f). c-Myc was the top gene strongly induced in HR6 cells compared with BT474T cells, which was controlled by ZMYND8 (Fig. 4a–c). c-Myc is known to be induced by BRD4[26]. We previously showed that ZMYND8 and BRD4 cooperate to activate hypoxia response in breast cancer[8]. To determine whether ZMYND8 induces c-Myc through BRD4, we treated BT474T cells overexpressing ZMYND8 or EV with a BRD4 inhibitor JQ-1 (1 μM) or vehicle for 6 hr. JQ-1 treatment significantly diminished ZMYND8-induced c-Myc expression at both mRNA and protein levels in BT474T cells (Supplementary Fig. 7a, b). These results indicate that ZMYND8 induces c-Myc expression through BRD4 in HER2+ breast cancer.

c-Myc amplification has been reported in trastuzumab resistant HER2+ breast tumors, but its role in trastuzumab resistance remains controversial[27–29]. To determine whether c-Myc regulates trastuzumab resistance in HER2+ breast tumors, we overexpressed c-Myc in trastuzumab-responsive BT474T and SK-BR-3 cells and found that c-Myc OE rendered these cells resistant to trastuzumab (Fig. 4d-f and Supplementary Fig. 8a–c). We next depleted c-Myc in HR6 cells by either of two independent sgRNAs. In contrast to c-Myc gain-of-function, c-Myc KO1 or KO2 robustly re-sensitized HR6 cells to 0.25 μg/mL trastuzumab (Fig. 4g-i). Similar results were observed when c-Myc KO1 or KO2 cells were treated with 0.2 μg/mL trastuzumab and/or 50 μg/mL pertuzumab (Supplementary Fig. 8d, e). In line with genetic loss-of-function studies, pharmacological inhibition of c-Myc with a small molecule inhibitor MYCi361 showed a synergistic growth inhibition of HR6 cells in a dose-dependent manner when combined with 0.25 μg/mL trastuzumab (Fig. 4j, k). Similarly, the combined treatment of 4 μM MYCi361 and 20 μg/mL trastuzumab robustly inhibited growth of tumor organoids, while their single treatment or combined treatment with lower doses of trastuzumab had no effect on organoid viability (Fig. 4l-s). MYCi361 treatment also re-sensitized tumor organoids to 5 μg/mL trastuzumab plus 50 μg/mL pertuzumab (Fig. 4p–s).

To determine if ZMYND8 drives trastuzumab resistance through c-Myc, we restored c-Myc expression in ZMYND8 KO1 HR6 cells by lentiviral transduction (Fig. 5a) and then assessed whether c-Myc re-expression abolishes the effect of ZMYND8 KO on trastuzumab sensitization. Trastuzumab treatment effectively reduced ZMYND8 KO1 colony growth, which was blocked by c-Myc expression (Fig. 5b, c). Given that ZMYND8 protein was induced by c-Myc (Fig. 4d and Supplementary Fig. 8a), we also restored ZMYND8 expression in c-Myc KO1 HR6 cells and found that ZMYND8 expression did not antagonize c-Myc KO to restore trastuzumab resistance (Fig. 5d–f). To determine the c-Myc rescue effect in vivo, we next implanted HR6, ZMYND8 KO1, and ZMYND8 KO1+c-Myc cells into the mammary fat pad of female NSG mice and mice were administrated with vehicle or 10 mg/kg trastuzumab once the tumor volume reached ~100 mm^3. As expected, ZMYND8 KO1 overcame HR6 tumor resistance to trastuzumab treatment. However, the expression of c-Myc restored growth of ZMYND8 KO1 tumors and partially blocked the antagonizing action of ZMYND8 KO1 on trastuzumab resistance in mice (Fig. 5g, h). Collectively, these findings indicate that c-Myc is a downstream effector of ZMYND8 driving trastuzumab resistance in HER2+ breast tumors.

https://doi.org/10.1038/s41467-025-59184-5

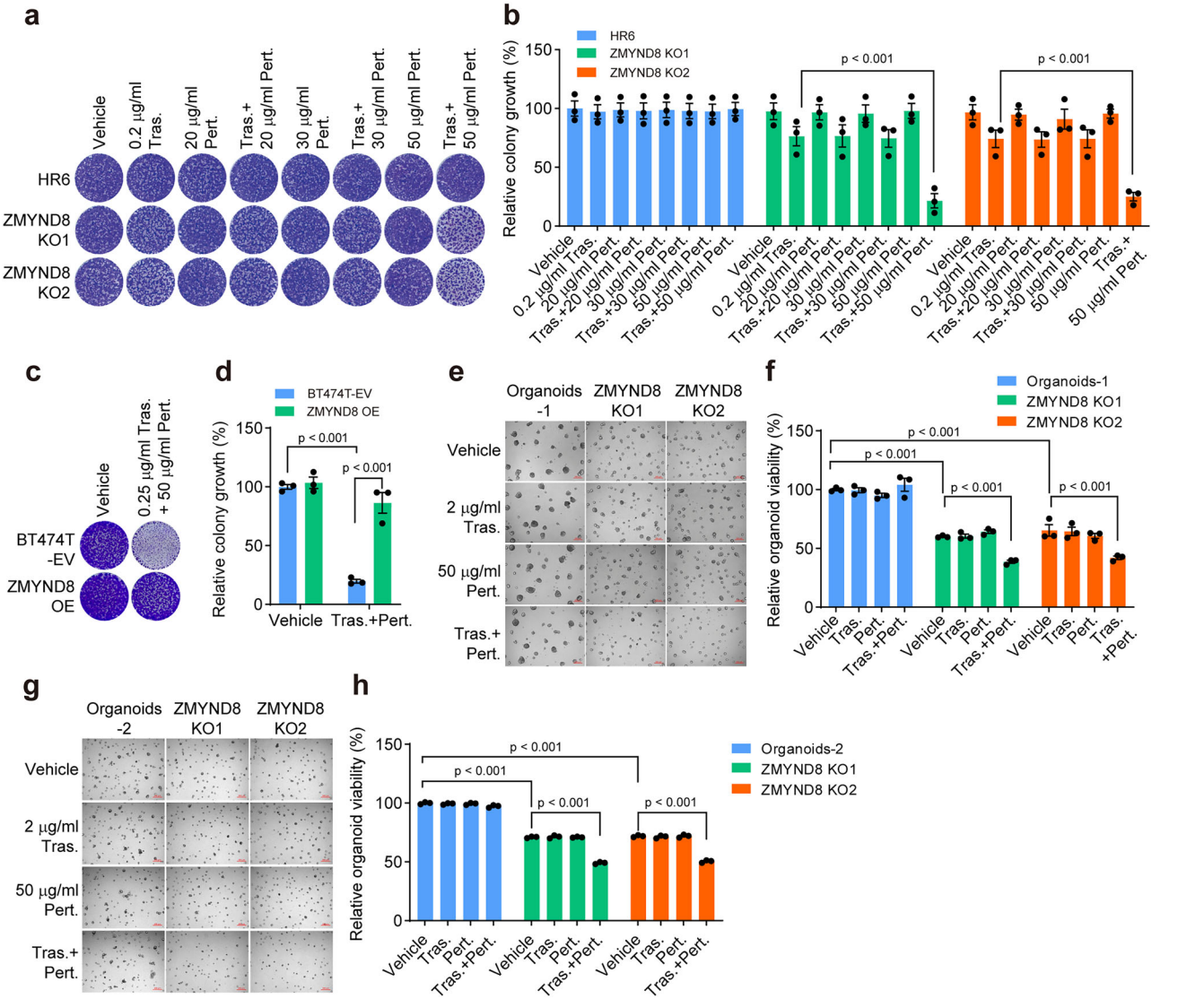

Fig. 2 | ZMYND8 drives trastuzumab plus pertuzumab resistance in HER2+ breast cancer in vitro. a, **b** Clonogenic growth of parental, ZMYND8 KO1 and KO2 HR6 cells treated with trastuzumab (Tras.), pertuzumab (Pert.), or trastuzumab +pertuzumab (Tras.+Pert.) for 6 days. Representative colony images (**a**) and quantification (**b**, $n = 3$). **c**, **d** Clonogenic growth of EV and ZMYND8 overexpressed BT474T cells treated with vehicle or trastuzumab+pertuzumab for 6 days. Representative colony images (**c**) and quantification (**d**, $n = 3$). **e**–**h** Growth of parental, ZMYND8 KO1 and KO2 organoids treated with vehicle, trastuzumab, pertuzumab, or trastuzumab+pertuzumab for 9 days. Representative organoid images (**e, g**) and organoid viability quantification (**f**, **h**, $n = 3$). Data from biological replicates represent mean ± SEM. *P*-value was determined by two-way ANOVA with Tukey's test (**b**, **d**, **f**, and **h**). Scale bar, 200 μm. Source data are provided as a Source Data file.

The ZMYND8-c-Myc axis alters cPLA2α-dependent glycerophospholipid metabolism in resistant HER2+ breast cancer

Recent studies suggest a role of metabolic reprogramming in trastuzumab resistance, although the underlying mechanism remains unknown[30,31]. c-Myc is a master regulator of cancer cell metabolism and regulates therapy resistance[19,32]. Thus, we hypothesized that ZMYND8 drives HER2 antibody resistance through c-Myc-induced metabolic alterations. To this end, we unbiasedly quantified the global metabolites in isogenic BT474T, HR6, and ZMYND8 KO1 or KO2 HR6 cells by mass spectrometry. 72 metabolites were significantly altered in either of 4 groups ($p < 0.05$, Supplementary Fig. 9a). Amongst these metabolites, multiple PC species were significantly increased in HR6 cells (fold change > 1.3), which was reversed by ZMYND8 KO1 or KO2 (Supplementary Fig. 9a). Pathway enrichment analysis revealed that only phospholipid biosynthesis was significantly enriched in HR6 cells (Supplementary Fig. 9b). To validate these results, we next quantified phospholipids in a comprehensive way with a modified and specific mass spectrometry approach in isogenic BT474T and HR6 cells. Levels of multiple glycerophospholipid species including PC, phosphatidylserine (PS), phosphatidylglycerol (PG), and lysophosphatidylcholine (LPC) were significantly increased by more than 1.5-fold in resistant HR6 cells compared with BT474T cells ($p < 0.001$, Fig. 6a). In contrast, DAG and TAG species were significantly decreased in HR6 cells ($p < 0.01$, Fig. 6a). Notably, alterations of PC, PS, DAG, and TAG species were reversed by either ZMYND8 KO1 or KO2 or c-Myc KO1 or KO2 ($p < 0.05$, Fig. 6a). These results indicate that both ZMYND8 and c-Myc are responsible for elevated PC and PS species and reduced DAG and TAG species in HER2 antibody resistant breast tumor cells.

To determine the mechanism underlying ZMYND8/c-Myc-induced glycerophospholipid alterations, we analyzed the expression of metabolic genes involved in PC and PS metabolism in our RNA-seq dataset. The PC biosynthesis gene *LPCAT1* and many phospholipases including *PLA2G2A*, *PLA2G2F*, *PLA2G3*, *PLA2G4A*, *PLA2G4F*, *PLA2G6*, *PLB1*, *PLBD1*, *PLCB1*, *PLCD3*, *PLCD4*, and *PLCE1* were significantly dysregulated in HR6 cells compared with BT474T cells, with *PLA2G3* and *PLA2G4A* dependent on ZMYND8 (Fig. 6b). RT-qPCR validated the specific induction of

https://doi.org/10.1038/s41467-025-59184-5

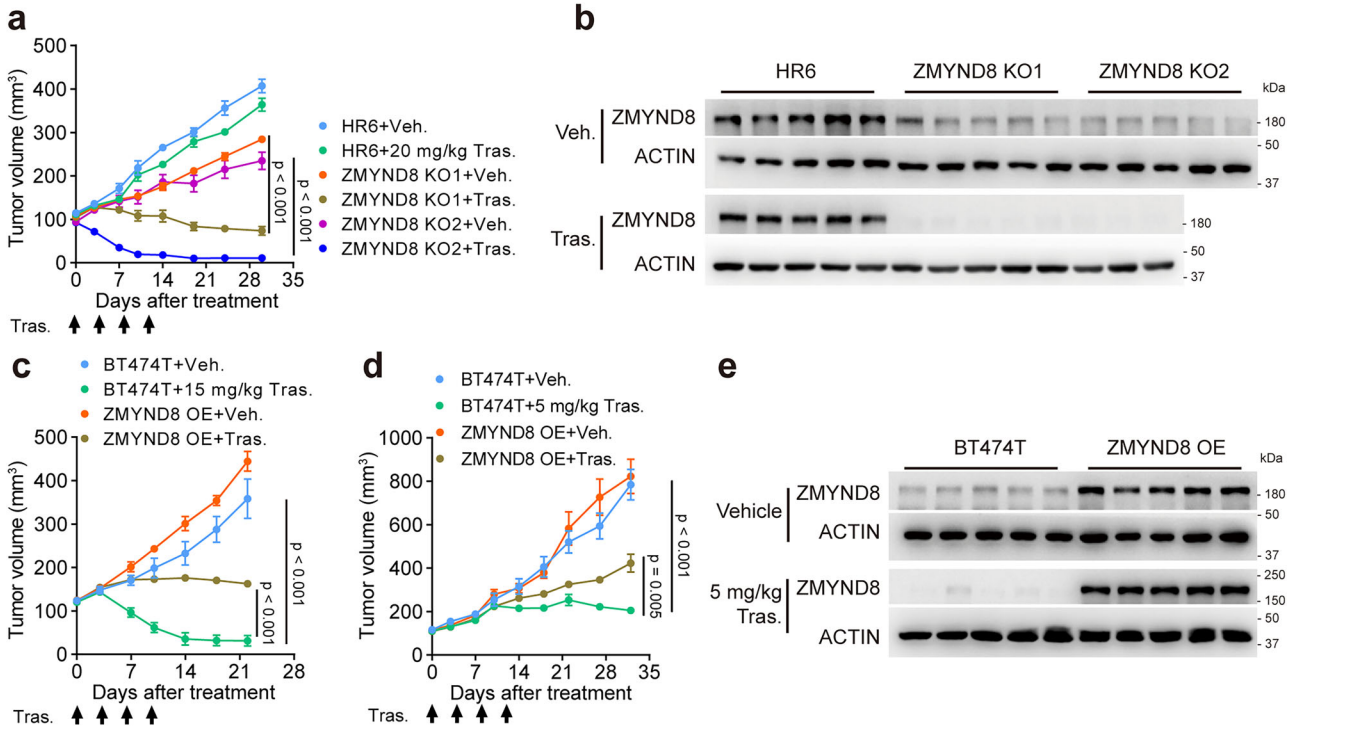

Fig. 3 | ZMYND8 drives trastuzumab resistance in HER2+ breast cancer in mice. **a** Growth curve of parental, ZMYND8 KO1 and ZMYND8 KO2 HR6 tumors in mice ($n = 5$) treated with vehicle (Veh.) or trastuzumab (Tras.). **b** Immunoblot analysis of ZMYND8 in treated tumors. **c**, **d** Growth curve of parental and ZMYND8 overexpressed BT474T tumors in mice ($n = 5$) treated with vehicle or trastuzumab at the dose of 15 mg/kg (**c**) or 5 mg/kg (**d**). **e** Immunoblot analysis of ZMYND8 in treated tumors. Data from biological replicates represent mean ± SEM. *P*-value was determined by two-way ANOVA with Tukey's test (**a**, **c**, and **d**). Source data are provided as a Source Data file.

PLA2G4A mRNA only by ZMYND8 in HR6 cells (Fig. 6c). Consistently, *PLA2G4A* mRNA was robustly increased by 2.2-fold in human HER2+ breast tumors after neoadjuvant treatment in the PAMELA clinical trial[25] ($n = 91$, Fig. 6d). *PLA2G4A* encodes cPLA2α protein, a member of the cytosolic calcium-dependent PLA2 group IV family that catalyzes the hydrolysis of glycerophospholipids[22]. We further found that ZMYND8 was required for cPLA2α protein induction in HR6 cells (Fig. 6e). cPLA2α mRNA and protein expression were also induced by c-Myc in HR6 cells (Fig. 6f, g). Notably, re-expression of c-Myc rescued cPLA2α protein levels in ZMYND8 KO1 HR6 cells (Fig. 6h), suggesting that ZMYND8 induces cPLA2α expression through c-Myc. To determine if *PLA2G4A* is a direct c-Myc target gene, we analyzed the *PLA2G4A* promoter and identified a putative c-Myc binding E-box element 5′-CACGTG-3′ (Fig. 6i). Chromatin immunoprecipitation (ChIP)-qPCR assay showed that c-Myc bound the E-box element at the *PLA2G4A* promoter in HR6 cells (Fig. 6j). In contrast, there was no direct binding of ZMYND8 to the *PLA2G4A* promoter (Fig. 6k). In line with these results, mRNA expression correlation analysis revealed a positive correlation between *MYC* and *PLA2G4A* in HER2+ tumors resistant to neoadjuvant double HER2 blockade in the PAMELA clinical trial (Supplementary Fig. 10a). However, *ZMYND8* mRNA did not correlate with *MYC* or *PLA2G4A* mRNA (Supplementary Fig. 10b, c), which may be due to the fact that ZMYND8 protein levels, rather than mRNA levels, were induced in resistant tumors (Fig. 1a and Supplementary Fig. 1f). Together, these findings indicate that the ZMYND8-c-Myc axis induces cPLA2α expression in breast cancer cells resistant to HER2 antibodies.

To determine if cPLA2α is responsible for ZMYND8/c-Myc-induced glycerophospholipid alterations, we quantified glycerophospholipids in isogenic BT474T, HR6, and cPLA2α KO1 or KO2 HR6 cells by mass spectrometry. Loss of cPLA2α prevented increases in PC and PS species but did not alter LPC and PG species in HR6 cells ($p < 0.01$, Fig. 6a). Reduction of DAG and TAG species was also reversed by cPLA2α KO in HR6 cells ($p < 0.05$, Fig. 6a). Consistently, pharmacological inhibition of cPLA2α with CDIBA (20 μM) significantly reduced PC species but increased TAG species in tumor organoids ($p < 0.01$, Fig. 6l). Together, these results indicate that the ZMYND8-c-Myc-cPLA2α axis reprograms PC, DAG, and TAG species in breast cancer resistant to HER2 antibodies.

Next, we examined whether cPLA2α drives HER2 antibody resistance. We depleted cPLA2α by either of two independent sgRNAs in HR6 cells (Fig. 7a). cPLA2α KO1 or KO2 re-sensitized HR6 cells to 0.25 μg/mL trastuzumab (Fig. 7b, c). Similar results were found in HR6 cells treated with 0.2 μg/mL trastuzumab plus 50 μg/mL pertuzumab (Fig. 7d, e). To determine whether the catalytic activity of cPLA2α is required for trastuzumab resistance, we re-introduced wildtype (WT) cPLA2α or its catalytically inactive mutant S505A into cPLA2α KO1 HR6 cells (Fig. 7f). Expression of WT cPLA2α in cPLA2α KO1 HR6 cells fully restored trastuzumab resistance, whereas S505A mutant failed to do so (Fig. 7g, h). Consistently, CDIBA dose-dependently reduced HR6 colony growth when combined with 0.25 μg/mL trastuzumab, though its single treatment had a marginal effect (Fig. 7i, j). Likewise, resistant organoids were re-sensitized to 20 μM CDIBA and 20 μg/mL trastuzumab combo, but not to CDIBA alone or 5 μM CDIBA and 20 μg/mL trastuzumab combo (Fig. 7k–n). Adding 20 μM CDIBA to 5 μg/mL trastuzumab plus 50 μg/mL pertuzumab combo also effectively reduced viability of resistant organoids (Fig. 7o–r). In vivo xenograft studies further showed that cPLA2α KO1 or KO2 inhibited HR6 tumor growth and robustly overcame trastuzumab resistance in NSG mice (Fig. 7s–u). Collectively, these results indicate that cPLA2α induced by the ZMYND8-c-Myc axis drives HER2 antibody resistance in vitro and in mice.

IL-27 induction by the ZMYND8-c-Myc-cPLA2α axis drives anti-HER2 therapy resistance in HER2+ breast cancer

Next, we assessed whether cPLA2α induces the expression of proinflammatory genes leading to ZMYND8/c-Myc-mediated HER2 antibody

https://doi.org/10.1038/s41467-025-59184-5

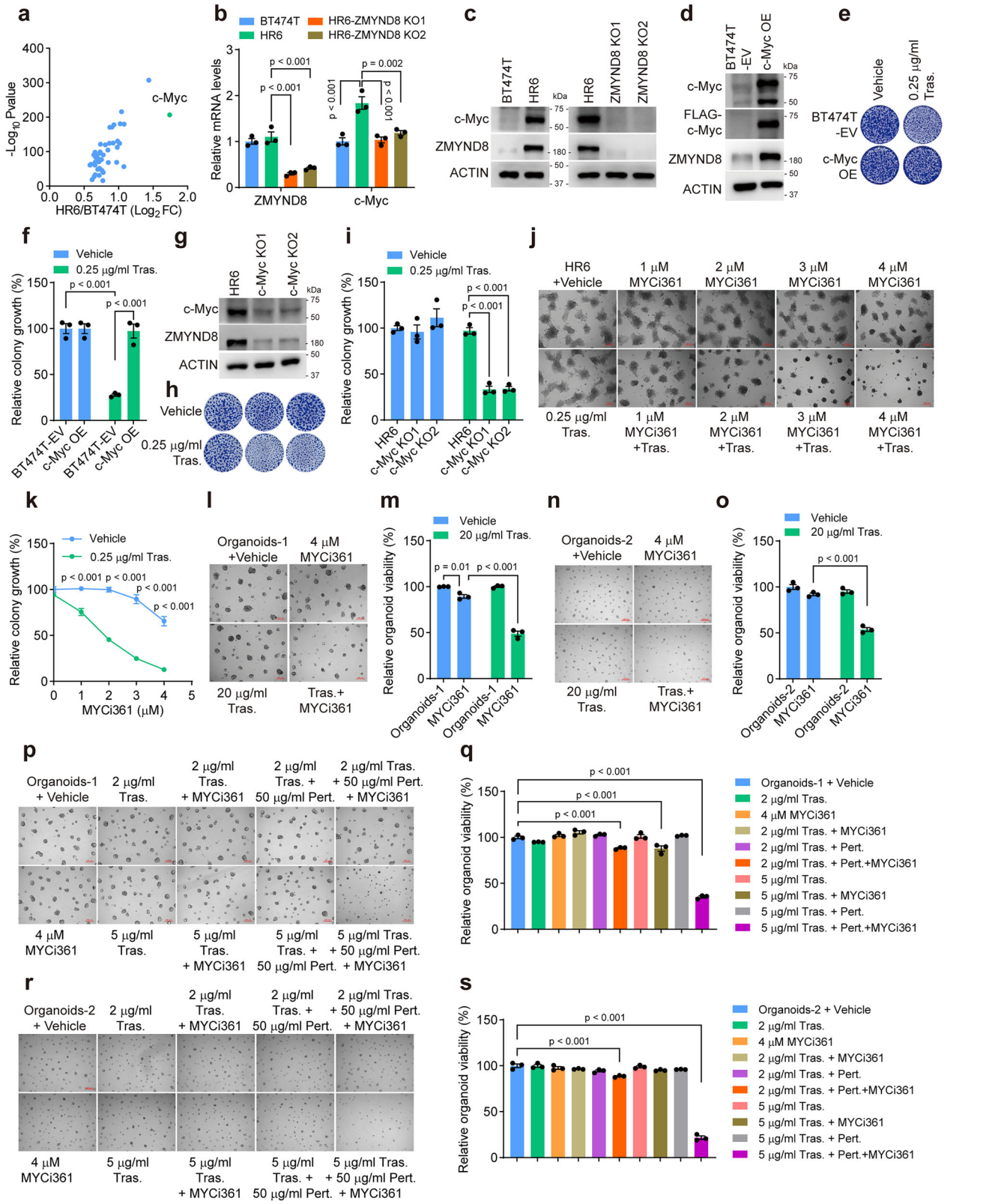

resistance. Proinflammatory genes dysregulated in our RNA-seq dataset were chosen for RT-qPCR validation with a goal of identifying proinflammatory genes induced by the ZMYND8-c-Myc-cPLA2α axis in HR6 cells. Amongst 11 proinflammatory genes, only *IL27* was induced by ZMYND8 in HR6 cells compared with BT474T cells (Fig. 8a), whereas other cytokines or chemokines were repressed or not regulated by ZMYND8 (Fig. 8a), consistent with our previous findings[13]. IL-27 protein secretion was attenuated by genetic loss of ZMYND8 or c-Myc or pharmacological inhibition of c-Myc in HR6 cells and tumor organoids (Fig. 8b–d). In line with this, *IL27* mRNA was increased by 2-fold in HER2+ breast tumors after neoadjuvant double HER2 blockade in the PAMELA clinical trial[25] (Fig. 8e). Next, we studied whether cPLA2α controls IL-27 secretion in resistant tumor cells. KO of cPLA2α reduced IL-27 mRNA and protein levels in HR6 cells, which was rescued

https://doi.org/10.1038/s41467-025-59184-5

Fig. 4 | c-Myc drives HER2 antibody resistance in HER2+ breast cancer in vitro. **a** mRNA levels of c-Myc and its target genes induced in HR6 cells compared with BT474T cells ($n = 2$). **b**, **c** RT-qPCR (**b**) and immunoblot (**c**) analyses of ZMYND8 and c-Myc in BT474T, HR6, ZMYND8 KO1 HR6, and ZMYND8 KO2 HR6 cells ($n = 3$). **d** Immunoblot analysis of ZMYND8 and c-Myc in BT474T cells expressing EV or c-Myc ($n = 3$). **e**, **f** Clonogenic growth of EV and c-Myc overexpressed BT474T cells treated with vehicle or trastuzumab (Tras.) for 6 days. Representative colony images (**e**) and quantification (**f**, $n = 3$). **g** Immunoblot analysis of ZMYND8 and c-Myc in parental and c-Myc KO1 or KO2 HR6 cells ($n = 3$). **h**, **i** Clonogenic growth of parental and c-Myc KO1 or KO2 HR6 cells treated with vehicle or trastuzumab for 6 days. Representative colony images (**h**) and quantification (**i**, $n = 3$). **j**, **k** Clonogenic growth of HR6 cells treated with vehicle, MYCi361, trastuzumab, or MYCi361+trastuzumab for 6 days. Representative colony images (**j**) and quantification (**k**, $n = 3$). **l**–**o** Growth of tumor organoids treated with vehicle, trastuzumab, MYCi361, or trastuzumab+MYCi361 for 9 days. Representative organoid images (**l**, **n**) and organoid viability quantification (**m**, **o**, $n = 3$). **p**–**s** Growth of tumor organoids treated with vehicle, trastuzumab, MYCi361, trastuzumab+pertuzumab, trastuzumab+MYCi361, or trastuzumab+pertuzumab+MYCi361 for 9 days. Representative organoid images (**p**, **r**) and organoid viability quantification (**q**, **s**, $n = 3$). Data from biological replicates represent mean ± SEM. *P*-value was determined by bioinformatics with edgeR (**a**), one-way ANOVA with Dunnett's test (**b**) or Tukey's test (**q**, **s**), or two-way ANOVA with Tukey's test (**f**, **i**, **k**, **m**, and **o**). Scale bar, 200 μm. Source data are provided as a Source Data file.

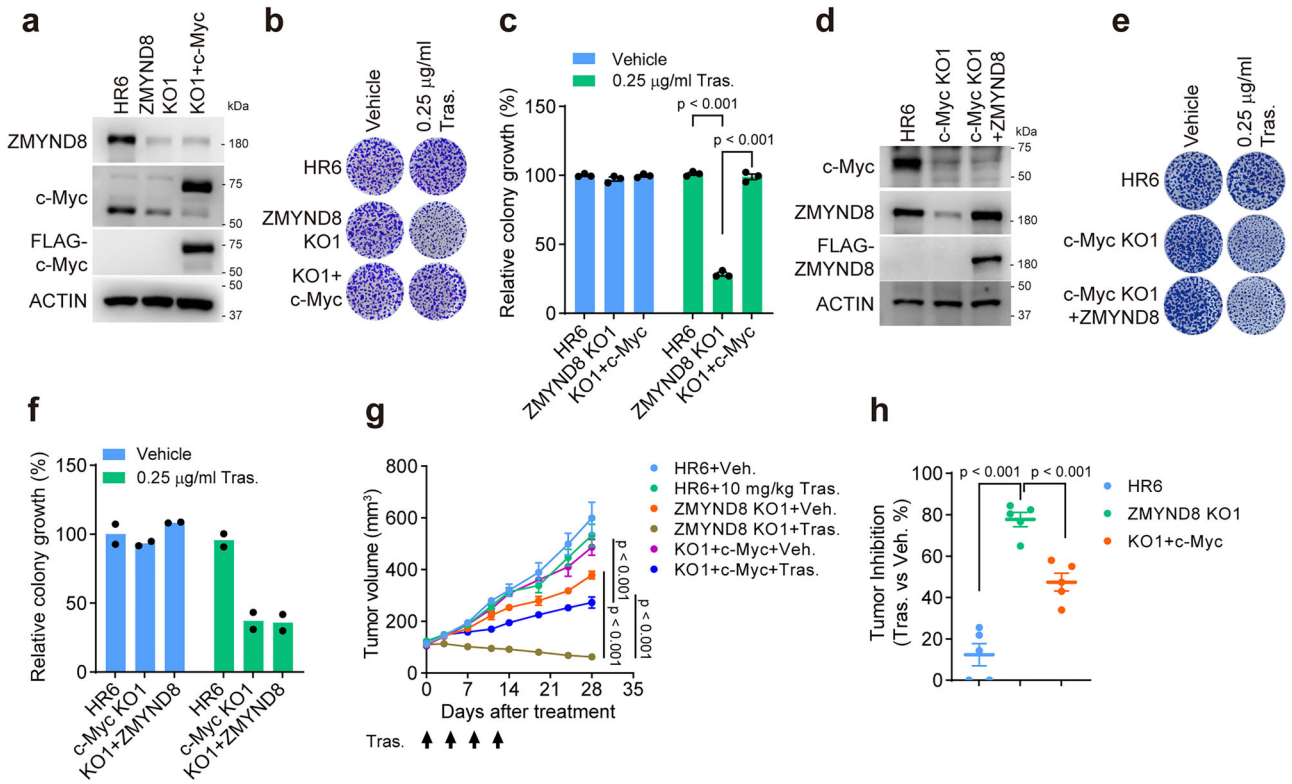

Fig. 5 | c-Myc is required for ZMYND8-induced trastuzumab resistance. **a** Immunoblot analysis of c-Myc and ZMYND8 proteins in parental, ZMYND8 KO1 and ZMYND8 KO1+c-Myc HR6 cells ($n = 3$). **b**, **c** Clonogenic growth of parental, ZMYND8 KO1 and ZMYND8 KO1+c-Myc HR6 cells treated with vehicle or trastuzumab for 6 days. Representative colony images (**b**) and quantification (**c**, $n = 3$). **d** Immunoblot analysis of ZMYND8 and c-Myc in parental, c-Myc KO1, and c-Myc KO1 + ZMYND8 HR6 cells ($n = 2$). **e**, **f** Clonogenic growth of parental, c-Myc KO1, and c-Myc KO1 + ZMYND8 HR6 cells treated with vehicle or trastuzumab for 6 days. Representative colony images (**e**) and quantification (**f**, $n = 2$). **g**, **h** Growth of parental, ZMYND8 KO1 and ZMYND8 KO1+c-Myc HR6 tumors in mice treated with vehicle or trastuzumab. Tumor growth curve (**g**) and the percentage of tumor inhibition (**h**, $n = 5$). Data from biological replicates represent mean ± SEM. *P*-value was determined by one-way ANOVA with Dunnett's test (**h**) or two-way ANOVA with Tukey's test (**c** and **g**). Source data are provided as a Source Data file.

by cPLA2α WT but not S505A mutant (Fig. 8f, g), suggesting that the catalytic activity of cPLA2α is required for IL-27 protein secretion. Pharmacological inhibition of cPLA2α also dose-dependently reduced IL-27 protein secretion in resistant tumor organoids (Fig. 8h). These results indicate that the ZMYND8-c-Myc-cPLA2α axis induces IL-27 secretion in resistant HER2+ breast tumors, which requires the catalytic activity of cPLA2α.

To determine a role of IL-27 in trastuzumab resistance, we pretreated trastuzumab-sensitive BT474 and SK-BR-3 cells with IL-27 protein, followed by 0.25 or 2.5 μg/mL trastuzumab treatment. Clonogenic assay showed that IL-27 at the dose of 50 ng/mL and 100 ng/mL fully induced resistance of both BT474 and SK-BR-3 cells to trastuzumab (Fig. 8i–l). Consistently, a partial resistance to trastuzumab was observed in BT474 cells incubated with conditional media from HR6 cells but not ZMYND8 KO1 or KO2 counterparts (Fig. 8m, n). We next studied whether IL-27 secretion contributes to ZMYND8/c-Myc/cPLA2α-mediated HER2 antibody resistance. To this end, we supplemented IL-27 protein in cultured cPLA2α KO1 or KO2 HR6 cells before treatment of 0.25 μg/mL trastuzumab or vehicle. Supplementation with IL-27 protein dose-dependently reversed sensitivity of cPLA2α KO1 or KO2 HR6 cells to trastuzumab (Fig. 8o, p). Similarly, IL-27 protein dose-dependently counteracted cPLA2α inhibitor CDIBA to increase trastuzumab resistance in tumor organoids (Fig. 8q-t). Next, we compared the effect of IL-27, ZMYND8, c-Myc, and cPLA2α on HER2 antibody resistance. To this end, we generated IL-27 KO1 and KO2 HR6 cells (Supplementary Fig. 11a, b), and these cells, along with HR6 cells and ZMYND8, c-Myc, and cPLA2α KO counterparts, were treated with 0.25 μg/mL trastuzumab or vehicle. Individual KO of ZMYND8, c-Myc, cPLA2α, and IL-27 achieved a comparable sensitivity of HR6

https://doi.org/10.1038/s41467-025-59184-5

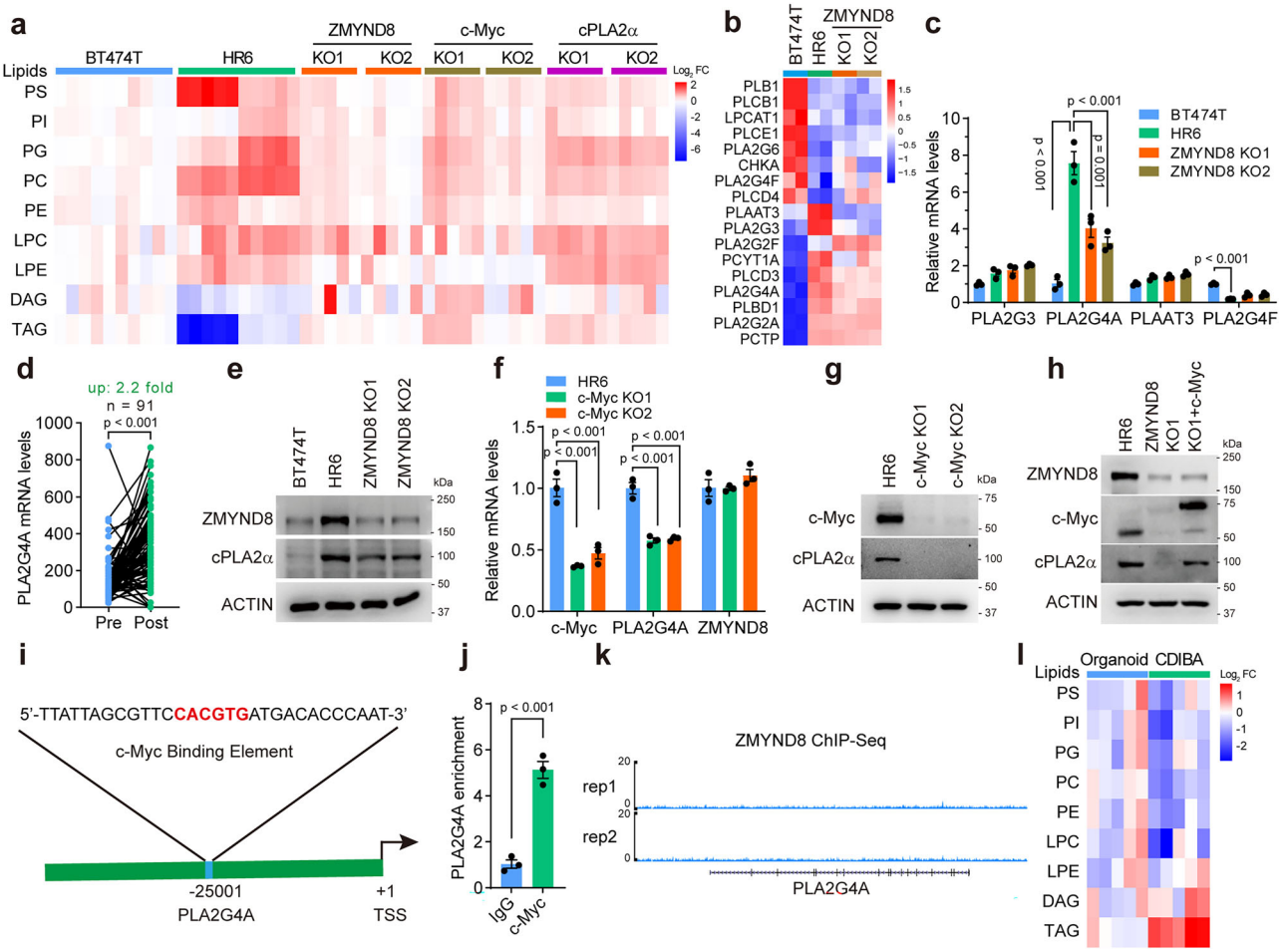

Fig. 6 | The ZMYND8-c-Myc axis alters glycerophospholipid metabolism in resistant HER2+ breast cancer via induction of cPLA2α. **a** Heatmap of glycerophospholipid species in BT474T ($n = 10$), HR6 ($n = 10$), ZMYND8 KO1 HR6 ($n = 5$), ZMYND8 KO2 HR6 ($n = 5$), c-Myc KO1 HR6 ($n = 5$), c-Myc KO2 HR6 ($n = 5$), cPLA2α KO1 HR6 ($n = 5$), and cPLA2α KO2 HR6 cells ($n = 5$). **b** Heatmap of expression of metabolic genes involved in glycerophospholipids in BT474T, HR6, ZMYND8 KO1 HR6, and ZMYND8 KO2 HR6 cells ($n = 2$). **c** RT-qPCR analysis of *PLA2G3*, *PLA2G4A*, *PLAAT3*, and *PLA2G4F* mRNAs in BT474T, HR6, ZMYND8 KO1 HR6, and ZMYND8 KO2 HR6 cells ($n = 3$). **d** Analysis of *PLA2G4A* mRNA expression in human HER2+ breast tumors before and after HER2-targeted therapy from the PAMELA clinical trial. **e** Immunoblot analysis of ZMYND8 and cPLA2α in BT474T, HR6, ZMYND8 KO1 HR6, and ZMYND8 KO2 HR6 cells ($n = 3$). **f** RT-qPCR analysis of *PLA2G4A*, *ZMYND8* and *MYC* mRNAs in parental, c-Myc KO1, and c-Myc KO2 HR6 cells ($n = 3$). **g** Immunoblot analysis of c-Myc and cPLA2α in parental, c-Myc KO1, and c-Myc KO2 HR6 cells ($n = 3$). **h** Immunoblot analysis of ZMYND8, c-Myc, and cPLA2α in parental, ZMYND8 KO1, and ZMYND8 KO1+c-Myc HR6 cells ($n = 3$). **i** Nucleotide sequence of the c-Myc binding element (in red) at the promoter of the *PLA2G4A* gene. **j** ChIP-qPCR assay with anti-c-Myc antibody or IgG in HR6 cells ($n = 3$). **k** Genome browser snapshot of ZMYND8 ChIP-seq in MDA-MB-231 cells (GSE108833). rep, replicate. **l** Heatmap of glycerophospholipid species in tumor organoids-1 treated with vehicle or CDIBA for 6 days ($n = 5$). Data from biological replicates represent mean ± SEM. *P*-value was determined by one-way ANOVA with Dunnett's test (**c** and **f**), paired 2-tailed Student's *t*-test (**d**), or unpaired 2-tailed Student's *t*-test (**j**). Source data are provided as a Source Data file.

cells to trastuzumab (Supplementary Fig. 11c, d). Similar results were observed when these cells were treated with 0.2 μg/mL trastuzumab plus 50 μg/mL pertuzumab (Supplementary Fig. 11e, f). These results support that ZMYND8, c-Myc, cPLA2α, and IL-27 work together within the same signaling axis to drive resistance to HER2 antibodies. Collectively, these findings indicate that IL-27 induced by the ZMYND8-c-Myc-cPLA2α axis drives HER2 antibody resistance in breast cancer.

cPLA2α induces IL-27 secretion through blocking DAG-induced activation of PKC

We next studied if the metabolite downstream of cPLA2α controls IL-27 secretion in drug resistant HER2+ breast tumors. AA (20-200 μM) failed to influence *IL27* levels in HR6 cells (Fig. 9a). Interestingly, supplementation with a cell membrane-permeable DAG analog, 1,2-Dioctanoyl-sn-glycerol (DOG), dose-dependently inhibited *IL27* mRNA expression in HR6 cells (Fig. 9b). DAG is generated from several precursors including glycerophospholipids, TAG, and phosphatidylinositol 4,5-bisphosphate by phospholipase C and D, sphingomyelin synthases, PA phosphohydrolases, and lipases[33]. However, none of these known DAG metabolic enzymes were altered and/or dysregulated by ZMYND8 in HR6 cells (Supplementary Fig. 6a), suggesting that these enzymes may not be involved in DAG reduction in resistant tumor cells. Phosphatidylcholine-specific phospholipase C (PC-PLC) is known to catalyze the hydrolysis of PC to DAG, although its coding gene has not been identified yet[34]. Treatment of a specific PC-PLC inhibitor D609 (20 or 50 μM) increased *IL27* mRNA in cPLA2α KO1 but not parental HR6 cells (Fig. 9c), suggesting that cPLA2α may competitively inhibit PC-PLC to block the hydrolysis of PC to DAG, leading to IL-27 secretion. We further showed that DOG treatment dose-dependently induced PKC phosphorylation (Fig. 9d), whereas AA (20-200 μM) failed to do so (Fig. 9e). In line with increased DAG, PKC phosphorylation was remarkably induced by cPLA2α KO1 or KO2 in HR6 cells (Fig. 9f), which was reversed by cPLA2α WT but not S505A mutant (Fig. 9g). Treatment of CDIBA similarly increased PKC phosphorylation in HR6 cells in a dose-dependent manner (Fig. 9h). Activation of PKC was blocked by

https://doi.org/10.1038/s41467-025-59184-5

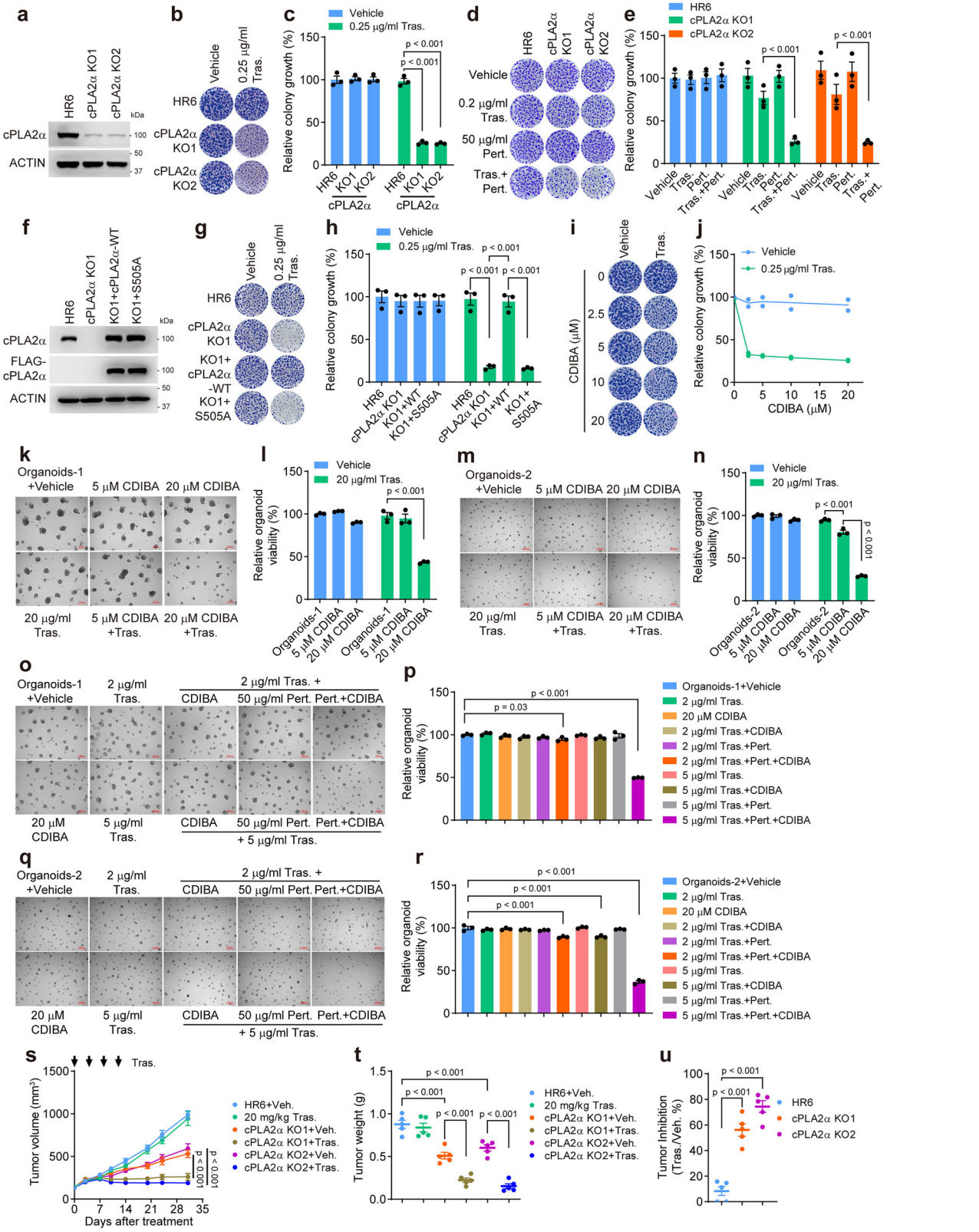

D609 treatment (20 or 50 μM) in cPLA2α KO1 HR6 cells (Fig. 9i), further supporting a signaling pathway that cPLA2α inactivates PC-PLC to decrease DAG and subsequent PKC inactivation in resistant HER2+ breast tumor cells. To determine whether the activity of PKC is required for IL-27 inhibition, we treated cPLA2α KO1 HR6 cells with a PKC inhibitor Go6983. Treatment of Go6983 dose-dependently abolished PKC phosphorylation and caused *IL27* derepression in cPLA2α KO1 HR6 cells (Fig. 9j, k). Consistently, trastuzumab resistance was restored in cPLA2α KO1 HR6 cells following D609 or Go6983 treatment (Fig. 9l–o). In line with IL-27 inhibition, DOG treatment dose-dependently sensitized HR6 cells to 0.25 μg/ml trastuzumab (Fig. 9p, q), but AA failed to do so (Fig. 9r, s). Together, these results indicate that reduction of DAG by cPLA2α inactivates PKC to induce IL-27 secretion in resistant HER2+ breast tumor cells.

Fig. 7 | cPLA2α drives HER2 antibody resistance in HER2+ breast cancer. **a**–**c** Clonogenic growth of parental, cPLA2α KO1, and cPLA2α KO2 HR6 cells treated with vehicle or trastuzumab (Tras.) for 6 days. Immunoblot analysis (**a**, $n = 3$), representative colony images (**b**), and quantification (**c**, $n = 3$). **d**, **e** Clonogenic growth of parental, cPLA2α KO1, and cPLA2α KO2 HR6 cells treated with vehicle, trastuzumab, pertuzumab (Pert.), or trastuzumab+pertuzumab for 6 days. Representative colony images (**d**) and quantification (**e**, $n = 3$). **f**–**h** Clonogenic growth of parental, cPLA2α KO1, cPLA2α KO1 + cPLA2α-WT and cPLA2α KO1 + S505A mutant HR6 cells treated with vehicle or trastuzumab for 6 days. Immunoblot analysis (**f**, $n = 3$), representative colony images (**g**), and quantification (**h**, $n = 3$). **i**, **j** Clonogenic growth of HR6 cells treated with vehicle, trastuzumab, CDIBA, or trastuzumab+CDIBA for 6 days. Representative colony images (**i**) and quantification (**j**, $n = 2$). **k**–**n** Growth of tumor organoids treated with vehicle, trastuzumab, CDIBA, or trastuzumab+CDIBA for 9 days. Representative organoid images (**k**, **m**) and organoid viability quantification (**l**, **n**, $n = 3$). **o**–**r** Growth of tumor organoids treated with vehicle, trastuzumab, CDIBA, trastuzumab+pertuzumab, trastuzumab+CDIBA, or trastuzumab+pertuzumab+CDIBA for 9 days. Representative organoid images (**o**, **q**) and organoid viability quantification (**p**, **r**, $n = 3$). **s**–**u** Growth of parental, cPLA2α KO1 and cPLA2α KO2 HR6 tumors in mice treated with vehicle or trastuzumab. Tumor growth curve (**s**), tumor weight (**t**), and the percentage of tumor inhibition (**u**, $n = 5$). Data from biological replicates represent mean ± SEM. *P*-value was determined by one-way ANOVA with Tukey's test (**p** and **r**) or Dunnett's test (**u**), or two-way ANOVA with Tukey's test (**c**, **e**, **h**, **l**, **n**, **s**, and **t**). Scale bar, 200 μm. Source data are provided as a Source Data file.

Targeting c-Myc or cPLA2α overcomes tumor resistance to HER2 antibodies in mice

We next assessed the therapeutic potential of MYCi361 and CDIBA on combating HER2 antibody resistance in vivo. To this end, HR6 cells were orthotopically implanted into the mammary fat pad of female NSG mice and mice were administrated intraperitoneally with trastuzumab (20 mg/kg), MYCi361 (50 mg/kg), or both when the tumor volume reached about 100 mm^3. MYCi361 treatment synergistically inhibited HR6 tumor growth when combined with trastuzumab, while its individual treatment had a modest inhibitory effect (Fig. 10a and Supplementary Fig. 12a, b). Combined treatment of MYCi361 and trastuzumab dramatically increased the levels of a cell death marker cleaved caspase-3 (CC3) but not a cell proliferation marker Ki67 in HR6 tumors (Fig. 10b–e). Likewise, 2 mg/kg CDIBA and 20 mg/kg trastuzumab combo also effectively increased CC3 levels and killed HR6 tumors in mice (Fig. 10f-h and Supplementary Fig. 12c, d). Notably, treatment of 50 mg/kg MYCi361 or 20 mg/kg CDIBA enhanced the response of human HER2+ PDX tumors to trastuzumab in mice (Fig. 10i–n and Supplementary Fig. 12e–h). MYCi361, CDIBA, trastuzumab, or their combos had little effect on mouse body weight, suggesting that mice are well tolerated with these treatments (Supplementary Fig. 12i–l). Lastly, we found that treatment of 50 mg/kg MYCi361 or 20 mg/kg CDIBA robustly increased CC3 levels and abrogated HER2+ PDX tumor resistance to 30 mg/kg trastuzumab plus 30 mg/kg pertuzumab in mice without obvious toxicities (Fig. 10o–q and Supplementary Fig. 12m–o). Both inhibitors significantly extended survival of tumor-bearing mice (Fig. 10r). Together, these findings indicate that targeting c-Myc or cPLA2α can effectively overcome anti-HER2 therapy resistance in the clinically relevant breast cancer mouse models.

Discussion

While several heterogenous trastuzumab resistance mechanisms have been previously proposed, the significant scientific barriers persist in designing the successful combination therapies capable of combating anti-HER2 therapy resistance in patients with breast cancer. In this study, we identified a signaling pathway driving HER2 antibody resistance in HER2+ breast cancer, which yields ZMYND8, c-Myc, cPLA2α, and IL-27 as druggable targets and biomarkers specifically for breast cancer resistant to trastuzumab and pertuzumab but not HER2 tyrosine kinase inhibitors (Fig. 10s). Importantly, our findings provide a proof-of-concept of c-Myc and cPLA2α inhibitor therapeutics as the rational strategies that can overcome resistance to anti-HER2 therapies (Fig. 10s). Therefore, this work has paved the way for a profound impact on both fundamental and translational aspects of human HER2+ breast cancer.

We showed that ZMYND8 is a key epigenetic regulator that initiates signal transduction of anti-HER2 therapy resistance by enhancing c-Myc transcription (Fig. 10s). ZMYND8's transcriptional coactivator function requires BRD4[8], which is known to control c-Myc transcription[35]. Interestingly, ZMYND8 is induced by HER2 targeted therapies at the protein but not mRNA levels in resistant HER2+ tumors. c-Myc controls ZMYND8 protein upregulation but the underlying mechanism requires further investigation. Nevertheless, these findings indicate a mutual regulation between ZMYND8 and c-Myc. c-Myc amplification has been detected in trastuzumab resistant human HER2+ breast tumors[27]. Our functional studies showed that both ZMYND8 and c-Myc are sufficient and necessary for acquired resistance to HER2 antibodies, highlighting the pivotal role of epigenetic dysregulation in anti-HER2 therapy resistance in breast cancer. Importantly, our present studies have expanded our understanding of ZMYND8 and c-Myc to the field of glycerophospholipid research. While ZMYND8 is known to regulate multiple signaling pathways in cancer cells[8,13–17], the ZMYND8-c-Myc axis is specific for HER2 antibody resistant breast cancer. Several intrinsic trastuzumab resistance mechanisms, including activation of PI3K/AKT and HER2 amplification, have been reported[3,7]. We found that ZMYND8 loss does not alter HER2 protein levels. However, whether ZMYND8 regulates additional intrinsic resistance mechanisms to HER2-targeted therapy needs to be explored in the future.

Our findings here provide the functional evidence of aberrant glycerophospholipid metabolism promoting anti-HER2 therapy resistance in breast cancer, which is supported by recent studies showing elevated lipid droplets in trastuzumab resistant HER2+ breast cancer cells[31]. Glycerophospholipids are previously reported to be elevated in HER2+ breast tumor cells[20], suggesting that increased glycerophospholipids prime breast tumor cells to develop an intrinsic resistance to anti-HER2 treatment. Previous studies demonstrated that HER2 OE increases fatty acid biosynthesis through stimulating the expression of fatty acid synthase[36]. However, HER2 expression is not altered in ZMYND8/c-Myc-overexpressed breast tumor cells. Notably, we uncover that cPLA2α is upregulated in HER2+ breast tumors from patients who do not respond to the dual HER2 blockade in the PAMELA trial and acts as a key regulator of aberrant glycerophospholipid metabolism and anti-HER2 therapy resistance in HER2+ breast cancer. cPLA2α is a primary phospholipase A2 that catalyzes the hydrolysis of glycerophospholipids to produce AA and lysophospholipids and also has phospholipase A1 activity under a certain condition[37]. Our studies suggest that cPLA2α may inactivate a currently unidentified PC-PLC, which requires its phospholipase A2 activity. As a result, activation of cPLA2α leads to a decrease in DAG production in resistant HER2+ breast tumor cells. These findings reveal a previously unappreciated function of cPLA2α in glycerophospholipid metabolism. Previous evidence has indicated that cPLA2α activation significantly correlates with HER2 overexpression[38], and that PIK3CA mutation is associated with increased cPLA2α activity[39]. These findings suggest that cPLA2α may be also involved in resistance to HER2-targeted therapies in tumors with HER2 amplification and/or PIK3CA mutation. Thus, our study may have important therapeutic implications for resistant tumors driven by HER2 amplification and/or PIK3CA mutation.

cPLA2α has been shown to promote metastasis of cancers, including triple-negative breast cancer and melanoma[23,40]. AA and lysophospholipids are primarily responsible for cPLA2α-mediated physiological and pathological processes[22]. Unexpectedly, we found

https://doi.org/10.1038/s41467-025-59184-5

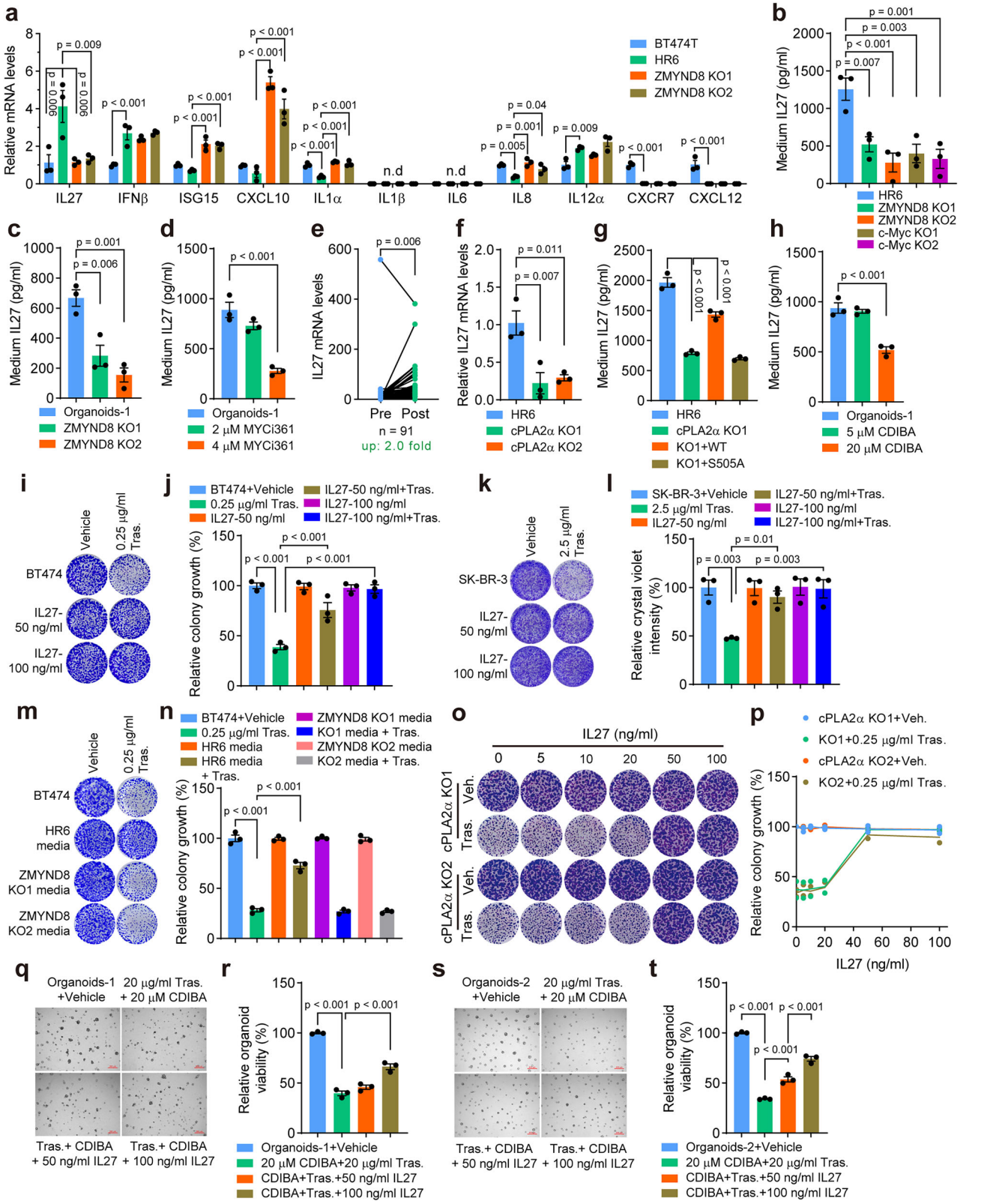

that, rather than AA, DAG negatively promotes resistance to HER2 antibodies in breast cancer through inhibiting inflammatory cytokine, providing insights into multifaceted regulation of inflammation by DAG. Recent mass spectrometry studies have revealed increased DAG species in breast tumor tissues compared to adjacent normal breast tissues, although their levels remain unknown in the HER2+ breast tumor subtype[41]. Given DAG's ability to enhance cytotoxic T cell-mediated antitumor immunity[42], our studies suggest that increasing DAG by cPLA2α inhibitor may yield a more robust impact on breast tumor sensitivity to HER2 antibodies in immunocompetent models, compared to what we have observed in immunodeficient mouse models. PKC plays a primary role in DAG-triggered signaling[42]. The PKC family consists of 10 isoforms with distinct functions[43]. Therefore, it is of high importance to identify the PKC isoform that is

https://doi.org/10.1038/s41467-025-59184-5

Fig. 8 | cPLA2α induces IL-27 secretion leading to HER2 antibody resistance in HER2+ breast cancer. a RT-qPCR analysis of indicated mRNAs in BT474T, HR6, ZMYND8 KO1 HR6, and ZMYND8 KO2 HR6 cells ($n = 3$). n.d, not detected. **b**, **c** ELISA analysis of IL-27 protein secretion from indicated cells and organoids ($n = 3$). **d** ELISA analysis of IL-27 protein secretion from tumor organoids treated with vehicle or MYCi361 ($n = 3$). **e** Analysis of *IL27* mRNA expression in human HER2+ breast tumors before and after HER2-targeted therapy from the PAMELA clinical trial. **f** *IL27* mRNA levels in parental, cPLA2α KO1 and KO2 HR6 cells ($n = 3$). **g** ELISA analysis of IL-27 protein secretion from parental, cPLA2α KO1, cPLA2α KO1 plus cPLA2α-WT or S505A HR6 cells ($n = 3$). **h** ELISA analysis of IL-27 protein secretion from tumor organoids treated with vehicle or CDIBA ($n = 3$). **i**–**l** Clonogenic growth of BT474 (**i**, **j**) and SK-BR-3 (**k**, **l**) cells pre-treated with IL-27 protein for 30 min followed by co-treatment with vehicle or trastuzumab (Tras.) for 6 days. Representative colony images (**i**, **k**) and quantification (**j**, **l**, $n = 3$). **m**, **n** Clonogenic growth of BT474 cells pre-treated with conditional media from HR6 cells or ZMYND8 KO counterparts for 30 min followed by co-treatment with vehicle or trastuzumab for 6 days. Representative colony images (**m**) and quantification (**n**, $n = 3$). **o**, **p** Clonogenic growth of cPLA2α KO1 and KO2 HR6 cells pre-treated with IL-27 protein for 30 min followed by co-treatment with vehicle or trastuzumab for 6 days. Representative colony images (**o**) and quantification (**p**, $n = 2$). **q**–**t** Growth of tumor organoids pre-treated with IL-27 protein for 30 min followed by co-treatment with vehicle or trastuzumab+CDIBA for 9 days. Representative organoid images (**q**, **s**) and organoid viability quantification (**r**, **t**, $n = 3$). Data from biological replicates represent mean ± SEM. *P*-value was determined by one-way ANOVA with Dunnett's test (**a**–**d**, **f**–**h**, **j**, **l**, **n**, **r**, and **t**), or paired 2-tailed Student's *t*-test (**e**). Scale bar, 200 μm. Source data are provided as a Source Data file.

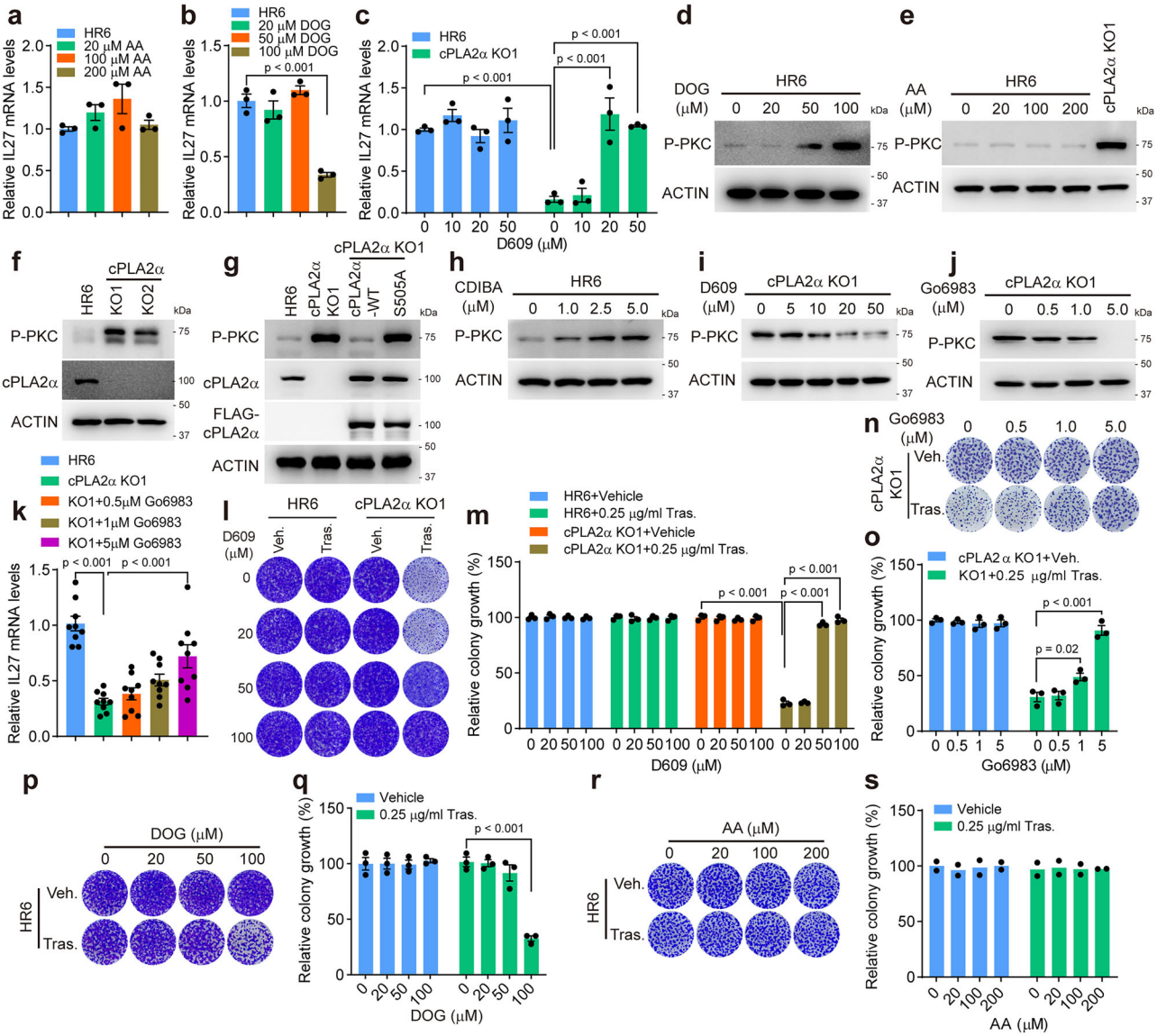

Fig. 9 | cPLA2α induces IL-27 secretion through blocking DAG-induced activation of PKC. a, **b** *IL27* mRNA levels in HR6 cells treated with AA (**a**) or DOG (**b**) for 3 days ($n = 3$). **c** *IL27* mRNA levels in parental and cPLA2α KO1 HR6 cells treated with D609 for 3 days ($n = 3$). **d**, **e** Immunoblot analysis of PKC phosphorylation (P-PKC) in HR6 cells treated with vehicle, DOG (**d**, $n = 3$), or AA (**e**, $n = 2$) for 3 days. cPLA2α KO1 HR6 cells as a positive control. **f**, **g** Immunoblot analysis of indicated protein in parental, cPLA2α KO1 or KO2, and rescued HR6 cells ($n = 3$). **h**–**j** Immunoblot analysis of P-PKC in indicated cells treated with vehicle, CDIBA (**h**, $n = 2$), D609 (**i**, $n = 2$), or Go6983 (**j**, $n = 2$) for 3 days. **k** *IL27* mRNA levels in parental and cPLA2α KO1 HR6 cells treated with vehicle or Go6983 for 3 days ($n = 9$). **l**–**s** Clonogenic growth of parental and cPLA2α KO1 HR6 cells pre-treated with vehicle, D609 (**l**, **m**, $n = 3$), Go6983 (**n**, **o**, $n = 3$), DOG (**p**, **q**, $n = 3$), or AA (**r**, **s**, $n = 2$) for 30 min followed by co-treatment with vehicle (Veh.) or trastuzumab (Tras.) for 6 days. Representative colony images (**l**, **n**, **p**, and **r**) and quantification (**m**, **o**, **q**, and **s**). Data from biological replicates represent mean ± SEM. *P*-value was determined by one-way ANOVA with Dunnett's test (**b**), or two-way ANOVA with Tukey's test (**c**, **k**, **m**, **o**, and **q**). Source data are provided as a Source Data file.

https://doi.org/10.1038/s41467-025-59184-5

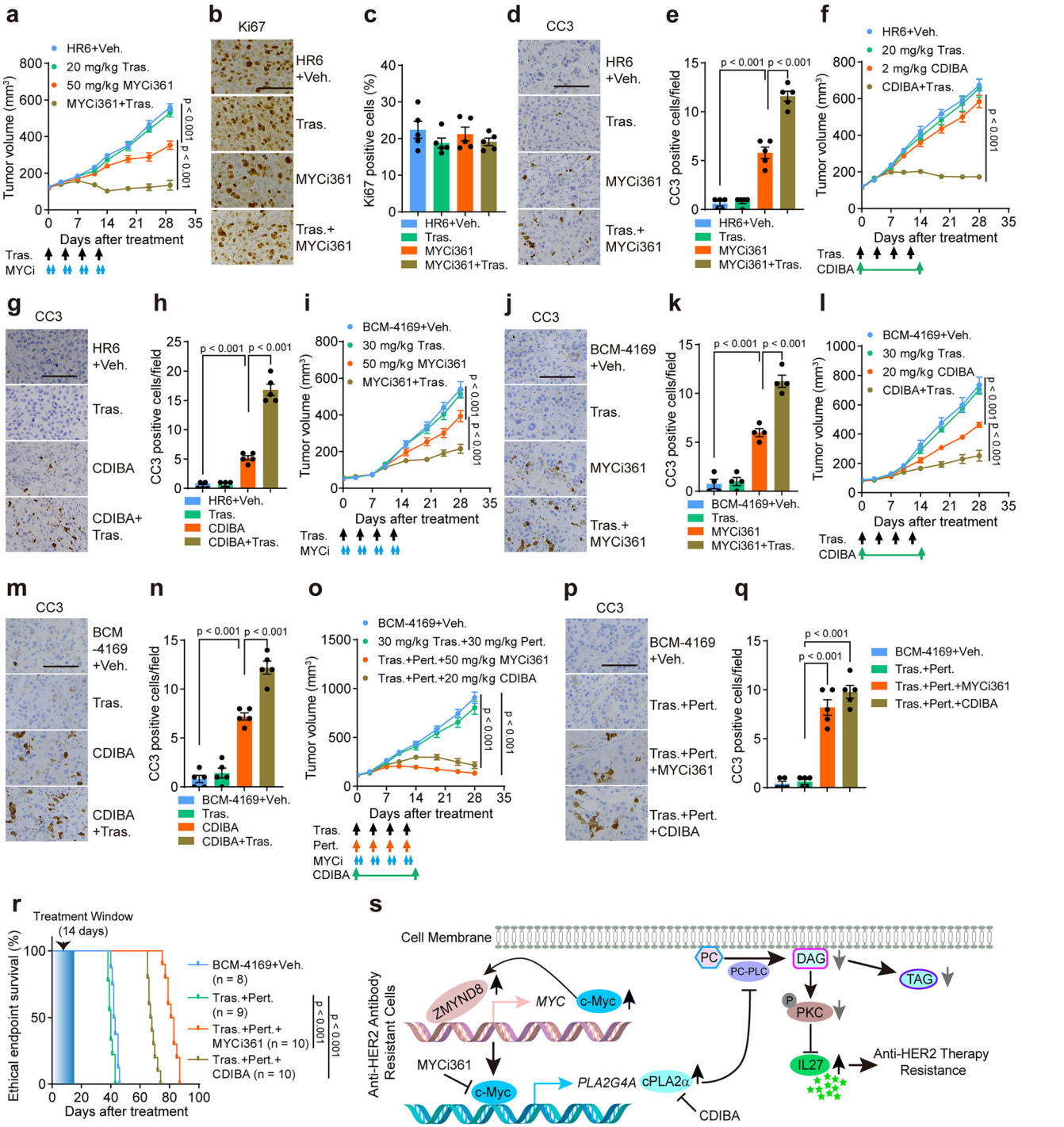

Fig. 10 | Targeting c-Myc or cPLA2α overcomes HER2 antibody resistance in mice. a Growth curve of HR6 tumors in mice treated with vehicle, trastuzumab (Tras.), MYCi361 (MYCi), or trastuzumab+MYCi361 ($n = 5$). **b**, **c** Representative Ki67 IHC image (**b**) and quantification (**c**) in tumors ($n = 5$). **d**, **e** Representative CC3 IHC image (**d**) and quantification (**e**) in tumors ($n = 5$). **f** Growth curve of HR6 tumors in mice treated with vehicle, trastuzumab, CDIBA, or trastuzumab+CDIBA ($n = 5$). **g**, **h** Representative CC3 IHC image (**g**) and quantification (**h**) in tumors ($n = 5$). **i** Growth curve of BCM-4169 tumors in mice treated with vehicle, trastuzumab, MYCi361, or trastuzumab+MYCi361 ($n = 4$). **j**, **k** Representative CC3 IHC image (**j**) and quantification (**k**) in tumors ($n = 4$). **l** Growth curve of BCM-4169 tumors in mice treated with vehicle, trastuzumab, CDIBA, or trastuzumab+CDIBA ($n = 5$). **m**, **n** Representative CC3 IHC image (**m**) and quantification (**n**) in tumors ($n = 5$). **o** Growth curve of BCM-4169 tumors in mice treated with vehicle, trastuzumab +pertuzumab (Pert.), trastuzumab+pertuzumab+MYCi361 or CDIBA ($n = 5$). **p**, **q** Representative CC3 IHC image (**p**) and quantification (**q**) in tumors ($n = 5$). **r** Kaplan–Meier survival curve of BCM-4169 tumor-bearing mice treated with vehicle, trastuzumab+pertuzumab, trastuzumab+pertuzumab+MYCi361 or CDIBA. **s** A working model of the ZMYND8-c-Myc-cPLA2α-IL-27 axis-induced anti-HER2 therapy resistance in HER2+ breast cancer. Data from biological replicates represent mean ± SEM. *P*-value was determined by one-way ANOVA with Dunnett's test (**q**) or Tukey's test (**e**, **h**, **k**, and **n**), two-way ANOVA with Tukey's test (**a**, **f**, **i**, **l**, and **o**), or log-rank test (**r**). Scale bar, 100 μm. Source data are provided as a Source Data file.

responsible for DAG-induced breast tumor sensitivity to anti-HER2 therapies.

HER2 expression is known to induce inflammation in breast cancer, which acts as a double-edged sword in a context-dependent manner. We showed that IL-27 plays an autocrine role in ZMYND8-c-Myc-cPLA2α-induced anti-HER2 antibody resistance in breast cancer (Fig. 10s). IL-27 belongs to the IL-6/IL-12 family that regulates inflammation and immune response[44]. Interestingly, we found that IL-27 is suppressed by PKC activation. While PKCα and PKCθ have been shown to induce IL-2, IL-12, and IL-27 in immune cells[45,46], PKCζ inhibits IL-6 and IL-12 expression and tumorigenesis by reducing histone acetylation[47]. Given that PKCα promotes trastuzumab resistance through activation of the ERK pathway in HER2+ breast cancer[48], our studies exclude a possible role of PKCα in IL-27 regulation. Previous studies demonstrate that IL-12 potentiates the antitumor effect of trastuzumab[49]. In contrast, IL-6 has been reported to induce trastuzumab resistance in HER2+ breast tumors[50]. These previous findings, along with ours, suggest a complex role of the IL-6/IL-12 family cytokines in anti-HER2 therapy resistance in breast cancer, potentially influenced by their upstream regulators and/or downstream effectors. IL-27 plays a critical context-dependent role in immune cells[51], which are enriched in the microenvironment of HER2+ breast tumors[52]. It is of high interest to comprehensively study the autocrine and/or paracrine effect of IL-27 on anti-HER2 therapy resistance in the preclinical animal models with proficient immune systems. IL-27 antibody has been shown to be well tolerated with a promising antitumor activity in patients with solid tumors in a phase I clinical trial (NCT04374877). Our findings suggest that neutralizing IL-27 with its antibody may be another effective strategy that can potentiate the current HER2-targeted therapies in breast cancer patients.

Methods

Study approval

Animal experiments were approved by the Animal Care and Use Committee at UT Southwestern Medical Center with the protocol number 2017-102199. The deidentified human tumor tissues, PDX, and organoids were approved by the Institutional Review Board at UT Southwestern Medical Center with written informed consent (STU082018-004).

Plasmid constructs

Human ZMYND8, c-Myc, cPLA2α, and IL-27 sgRNAs listed in Supplementary Table 2 were cloned into lentiCRISPR-V2 vector as described previously[8]. Human ZMYND8 and scrambled control (SC) shRNAs were cloned into pLKO.1 vector as described previously[8]. Human ZMYND8, c-Myc and cPLA2α cDNAs were cloned into pLVX-N-FLAG vector. Catalytically inactive S505 A mutant was generated by site-directed PCR mutagenesis. All plasmids were verified by DNA sanger sequencing.

Cell culture

Parental BT474 cells (from ATCC, HTB-20), isogenic BT474T and HR6 cells (from C.L.A), 5637 and 5637NR cells (from C.L.A), OVCAR8 and OVCAR8NR cells (from C.L.A), and SK-BR-3 cells (ATCC, HTB-30) were cultured in RPMI1640 or McCoy's 5A with 10% heat-inactivated fetal bovine serum (FBS, Sigma) at 37 °C in a 5% CO_2/95% air incubator. OVCAR8NR and 5637NR cells were maintained with 1000 nM and 600 nM neratinib, respectively. Trastuzumab (10 μg/mL) was added to HR6 cells for maintenance of resistance. ZMYND8, c-Myc, cPLA2α, and IL-27 KO or KD cells were freshly generated by lentiviral transduction of sgRNAs or shRNAs in the presence of 10 μg/mL polybrene (Sigma) and selected with puromycin (1 μg/mL). ZMYND8 or c-Myc overexpressed BT474T and SK-BR-3 cells were freshly generated by lentiviral transduction of ZMYND8 or c-Myc cDNA and selected with puromycin. ZMYND8-rescued HR6 cells were freshly generated by lentiviral transduction of ZMYND8 cDNA in ZMYND8 KD or c-Myc KO cells. c-Myc-rescued HR6 cells were freshly generated by lentiviral transduction of c-Myc cDNA in ZMYND8 KO cells. cPLA2α-WT and S505A mutant-rescued HR6 cells were freshly generated by lentiviral transduction of respective WT and S505A cPLA2α cDNA in cPLA2α KO cells. Cells within three passages were used for experiments. All cell lines were mycoplasma-free.

Clonogenic assay

HR6 (1.0×10^4 cells/well), ZMYND8 KO (1.5×10^4 cells/well), ZMYND8 KD (1.5×10^4 cells/well), ZMYND8 KD + ZMYND8 (1.0×10^4 cells/well), c-Myc KO (1.5×10^4 cells/well), ZMYND8 KO+c-Myc (1.5×10^4 cells/well), cPLA2α KO (1.0×10^4 cells/well) cells, BT474T (0.8-1.0 x 10^4 cells/well), BT474T-c-Myc OE (0.8×10^4 cells/well), BT474T-ZMYND8 OE (0.8×10^4 cells/well), BT474T-ZMYND8 KO ($1.0\text{-}2.0 \times 10^4$ cells/well), SK-BR-3 (0.5×10^4 cells/well), SK-BR-3-c-Myc OE (0.5×10^4 cells/well), SK-BR-3-ZMYND8 OE (0.5×10^4 cells/well), SK-BR-3-ZMYND8 KO ($0.5\text{-}1.5 \times 10^4$ cells/well), and BT474 (1.0×10^4 cells/well) cells were seeded onto a 96-well plate and cultured for 24 h and then treated with indicated drugs for 6 days. Colonies were fixed with 100% methanol for 15 min and stained with 0.1% crystal violet (MilliporeSigma). After staining, the colony area or crystal violet intensity was quantified[8]. Conditional media were generated from HR6 cells (3.0×10^5 cells/well) and ZMYND8 KO counterparts (5.0×10^5 cells/well) cultured for 3 days. 200 μL conditional media were added to BT474 cells 30 min before treatment with 0.25 μg/mL trastuzumab, and replaced every 3 days.

Cell migration assay

Cell migration assay was performed in 24-well plate with an 8 μm-pore Boyden chamber. 1×10^5 cells were seeded in serum-free medium in the upper chamber and allowed to migrate for 36 h toward the bottom chamber containing medium with 10% FBS. The migratory cells were fixed with 100% methanol, stained with 0.1% crystal violet, and imaged using a Zeiss Axio Observer Z1 fluorescence microscope. The number of migratory cells was counted from three independent microscope fields per sample.

Metabolomics assay

1×10^6 cells were cultured with fresh medium with dialyzed 10% FBS (MilliporeSigma) for 2 h and then rinsed once with 3 mL of ice-cold normal saline solution. Cells were lyzed with 500 μL of pre-cooled 80% (vol/vol) methanol in water and incubated for 5 min on ice. After scraping from the plate, the cell lysate/methanol mixture was transferred to a 1 mL Eppendorf tube. The tubes were frozen in liquid nitrogen and repeated for three freeze-thaw cycles between liquid nitrogen and 37 °C water. After the third thaw, the tubes were vortexed for 1 min, and then centrifuged at ~20,000 g for 15 min at 4 °C. The supernatant containing metabolites was carefully transferred into a new tube. Protein was quantified in the supernatant using the Pierce BCA kit. The supernatant equivalent to 10 μg of protein was transferred to a new Eppendorf tube and dried using a SpeedVac. The dried samples were resuspended in 100 μL acetonitrile/water 80:20 (vol/vol), vortexed rigorously for 1 min, and centrifuged at ~20,000 g for 15 min at 4 °C. After collecting the supernatant, metabolites were quantified by LC-MS. The heatmap was generated by the statistical analysis module on the MetaboAnalyst website.

Lipid profiling assay

250,000 cells were lysed at room temperature for lipid extraction using a modified methyl-tert-butyl ether method in a fresh 16 × 100 mm glass tube with a PTFE-lined cap (Fisher Scientific, Pittsburg, PA)[53]. After vortexing and centrifugation at 2,671 × *g* for 5 min, the organic phase was collected, spiked with 20 μL of a 1:5 diluted Splash Lipidomix standard solution (Avanti, Alabaster, AL), and dried

under N_2 air flow. The samples were resuspended in hexane and transferred to 1.5 mL amber GC vials. Lipids were analyzed by LC-MS/MS using a SCIEX QTRAP 6500+ (SCIEX, Framingham, MA) equipped with a Shimadzu LC-30AD (Shimadzu, Columbia, MD) high-performance liquid chromatography system and a 150 × 2.1 mm, 5 µm Supelco Ascentis silica column (Supelco, Bellefonte, PA). Samples were injected at a flow rate of 0.3 mL/min at 2.5% solvent B (methyl tert-butyl ether) and 97.5% Solvent A (hexane). Solvent B was increased to 5% over 3 min and then to 60% over 6 min. Solvent B was decreased to 0% during 30 s while Solvent C [90:10 (v/v) isopropanol-water] was set at 20% and increased to 40% during the following 11 min. Solvent C is increased to 44% over 6 min and then to 60% over 50 sec. The system was held at 60% solvent C for 1 min prior to re-equilibration at 2.5% of solvent B for 5 min at a 1.2 mL/min flow rate. Solvent D [95:5 (v/v) acetonitrile-water with 10 mM ammonium acetate] was infused post-column at 0.03 mL/min. Column oven temperature was 25 °C. Data was acquired in positive and negative ionization mode using multiple reaction monitoring and analyzed using MultiQuant software (SCIEX). The identified lipid species were normalized to its corresponding internal standard and protein concentration.

Immunoblot assay

Cells were lyzed with NETN lysis buffer (150 mM NaCl, 1 mM EDTA, 10 mM Tris-HCl, pH 8.0, 0.5% IGEPAL CA-630, and protease inhibitor cocktail), followed by sonication for 15 s. Cell lysis was resolved by sodium dodecyl sulfate-polyacrylamide gel electrophoresis and transferred to nitrocellulose membrane. The following primary antibodies were used: anti-ZMYND8 antibody (1:1000, A302-089A, Bethyl Laboratories), anti-c-Myc antibody (1:500, sc-40, Santa Cruz Biotechnology), anti-cPLA2α antibody (1:500, 2832S, Cell Signaling Technology), anti-HER2 antibody (1:1000, sc-33684, Santa Cruz Biotechnology), anti-FLAG (1:5000, F9291, Sigma), anti-P-PKC (1:500, 9371T, Cell Signaling Technology), and anti-β-actin (1:5000, 81115-1-RR, Proteintech). Proteins were visualized by chemiluminescence with ECL prime (GE Healthcare).

RT-qPCR assay

Total RNA was isolated from the cultured cells or tumor organoids with Trizol and treated with DNase I (ThermoFisher). First-strand cDNA was synthesized using the iScript cDNA synthesis kit (Bio-Rad). Real-time qPCR was performed[13] and data were normalized to RPL13A mRNA. qPCR primers used in this study are shown in Supplementary Table 3.

RNA-seq assay

Total RNA was isolated from the cultured cells using the RNeasy mini kit (Qiagen) and treated with DNase (Qiagen). mRNA was used for library preparation with the KAPA mRNA HyperPrep Kit (Roche) and sequenced on the Illumina NextSeq 500. Bioinformatics analysis was conducted using the Galaxy RNA-seq workflow. Fastq files were subjected to quality check using FastQC (Galaxy version 0.74 + galaxy0) and then trimmed using Trimmomatic (Galaxy version 0.39 + galaxy2). Trimmed fastq files were mapped to hg38 using HISAT2 (Galaxy version 2.2.1 + galaxy1). Duplicates were removed using MarkDuplicates (Galaxy version 3.1.1.0). Read counts were generated using featureCounts (Galaxy version 2.0.3 + galaxy2) and the differential expression analysis was performed using edgeR (Galaxy version 3.36.0 + galaxy4). The differential expression genes with a false discovery rate (FDR) < 0.05, logCPM > 0, and |fold change | > 2 as cutoff criteria were selected for the pathway analysis using GSEA (v4.3.3). The heatmap and bubble plots were generated with SRplot[54].

ChIP-qPCR assay

Cells were fixed in 10 mL of culture media containing 1% formaldehyde for 10 min at room temperature and quenched by addition of 1 mL of 2 M glycine. After washing with TBSE buffer (20 mM Tris-HCl, pH 7.5, 150 mM NaCl, 1 mM EDTA), cells were lysed in lysis buffer (10 mM Tris-HCl, pH 8.0, 100 mM NaCl, 10 mM EDTA, 0.25% Triton X-100, and protease inhibitor cocktail) and centrifuged. The nuclei pellet was collected and lysed in lysis buffer (50 mM HEPES-KOH, pH 7.5, 150 mM NaCl, 1 mM EDTA, 1% Triton X-100, 0.1% sodium deoxycholate, 1% SDS, and protease inhibitor cocktail) to extract chromatin. The chromatin DNA was fragmented by sonication and then centrifuged at 21,000 g for 30 min at 4 °C. The supernatant was diluted in ChIP immunoprecipitation buffer (50 mM HEPES-KOH, pH 7.5, 150 mM NaCl, 1 mM EDTA, 1% Triton X-100, 0.1% sodium deoxycholate, 0.1% SDS, and protease inhibitor cocktail) and then subjected to immunoprecipitation overnight in the presence of Dynabeads (ThermoFisher) with anti-c-Myc antibody (sc-40, Santa Cruz Biotechnology) or normal mouse IgG (sc-2025, Santa Cruz Biotechnology) at 4 °C. Beads were washed, eluted, and reverse-crosslinked at 65 °C for 4 h, followed by treatment with proteinase K at 45 °C for 1 h. The precipitated DNA was purified with MinElute PCR purification kit (Qiagen) and quantified by real-time qPCR assay. The primers used for ChIP-qPCR are listed in Supplementary Table 2. Fold enrichment was calculated based on Ct as $2^{-\Delta(\Delta Ct)}$, where $\Delta Ct = Ct_{IP} - Ct_{Input}$ and $\Delta(\Delta Ct) = \Delta Ct_{antibody} - \Delta Ct_{IgG}$.

IL-27 ELISA assay

HR6 cells (3.0×10^5 cells/well) as well as ZMYND8 KO (5×10^5 cells/well), c-Myc KO (5×10^5 cells/well), cPLA2α KO (3.0×10^5 cells/well), and IL-27 KO (3.0×10^5 cells/well) counterparts were seeded onto a 6-well plate with 1 mL of culture medium. Organoids (5.0×10^4 cells/well) were seeded onto a 48-well plate (pre-coated with 50 µL basement membrane extract) with 0.2 mL of culture medium and transduced with ZMYND8 sgRNA lentivirus or treated with MYCi361 (2 µM or 4 µM) or CDIBA (5 µM or 20 µM). Four days after culture, media were collected and subjected to IL-27 protein measurement with a human IL-27 ELISA kit (ThermoFisher) according to the manufacturer's instructions. The concentration of IL-27 protein was normalized to HR6 cell number or organoid viability.

Animal studies

Female mice were used in our study because we studied breast cancer in women. 1×10^6 HR6 or BT474T cells suspended in PBS/Matrigel (1:1, Corning) were implanted into the second left mammary fat pad of 6-8 week-old female NSG mice. Human HER2+ PDX tumors (8 mm^3) were implanted into the fourth left mammary fat pad of 6-8-week-old female NSG mice. Mice were subcutaneously administrated with 17β-estradiol (1 µmol per mouse) daily before the tumor volume reached to 100 mm^3, and then were intraperitoneally administrated with trastuzumab (5-30 mg/kg, twice per week for 2 weeks), trastuzumab plus pertuzumab (30 mg/kg, twice per week for 2 weeks), MYCi361 (50 mg/kg/day, 2 days on/2 days off for 4 rounds), or CDIBA (2–20 mg/kg, daily for 2 weeks). Tumor volume was measured as described previously[8]. About 2 weeks after drug treatment, tumors were harvested, imaged, and weighted. Mouse survival studies were terminated upon reaching a tumor length of 2 cm. The maximum tumor burden permitted by the Animal Care and Use Committee at UT Southwestern Medical Center is 2 cm in length. In this study, the length of all tumors did not exceed 2 cm. Mice were housed in groups of 4–5/cage, with temperatures ranging from 65-75 °F, humidity between 40-60%, and a 12 h light/12 h dark cycle.

IHC assay

IHC assay was performed on a Dako Autostainer Link 48 system[8]. The slides were baked, deparaffinized, and hydrated, followed by antigen retrieval in a Dako PT Link. The tissues were incubated with a peroxidase block and then a following primary antibody to detect the target antigen. The anti-ZMYND8 antibody (1:1500, A302-089A) was purchased from Bethyl Laboratories. The anti-Ki67 antibody (1:10000, 7309-1-AP) was purchased from Proteintech. The anti-CC3 antibody (1:

1500, 9661S) was purchased from Cell Signaling Technology. The EnVision FLEX visualization system (Agilent) was used to visualize the staining.

Patient-derived tumor organoids

Human metastatic HER2+ PDX tumors (BCM-4169 and HCI-032) were harvested from female NSG mice when the tumor volume reached to 500-600 mm^3. PDX tumors were washed twice with 10 mL of DMEM/F-12 medium supplemented with 1x GlutaMax, 10 mM HEPES, and 50 U/mL penicillin/50 µg/mL streptomycin/100 µg/mL neomycin and minced into small fragments. Tumor fragments were digested for 2 h in 10 mL of dissociation media (DMEM/F-12, 300 U/mL collagenase, 100 U/mL hyaluronidase, 10 ng/mL EGF, 1 mg/mL insulin) with constant shaking at 275 rpm at 37 °C, filtered through a 100-µm strainer, and centrifuged at 200 g for 5 min. The cell pellet was resuspended in 10 mL of red blood cell lysis buffer for 5 min at 37 °C and centrifuged at 200 g for 5 min. Cell dissociation was performed again by incubating cell pellets for 5 min with 3 mL pre-warmed trypsin in a 37 °C incubator, and terminated by 6 mL of neutralization solution (2% FBS in PBS). After centrifugation at 200 g for 5 min, tumor cells were counted and suspended with PBS containing 0.5% BSA. Mouse Cell Depletion Cocktail (Miltenyi Biotec, 130-104-694) was used to eliminate potential mouse cells from human tumor cells. Human tumor cells were resuspended in cold basement membrane extract and cell suspension was seeded to 24-well plate and solidified for 20 min at 37 °C. Tumor organoids-1 from BCM-4169 were cultured in DMEM/F-12 medium supplemented with 1/10 volume R-Spondin 1 media collected from R-Spondin1-expressing 293T cells, 5 nM NRG1, 5 ng/mL FGF7, 20 ng/mL FGF10, 5 ng/mL EGF, 100 ng/mL Noggin, 500 nM A83-01, 5 mM Y-27632, 500 nM SB202190, 1x B27 supplement, 1.25 mM N-Acetylcysteine, 5 mM Nicotinamide, 1x GlutaMax, 10 mM HEPES, and 50 U/mL penicillin/50 µg/mL streptomycin/100 µg/mL neomycin. Tumor organoids-2 from HCI-032 were cultured in DMEM/F-12 medium supplemented with 5% FBS, 1 µg/mL hydrocortisone, 10 ng/mL EGF, 10 µM Y-27632, 100 ng/mL FGF2, 1 mM N-Acetylcysteine, 10 nM NRG1, 10 mM HEPES, 1 x Glutamax, and 50 U/mL penicillin/50 µg/mL streptomycin/100 µg/mL neomycin. Organoids were cultured in a 5% CO_2/95% air incubator at 37 °C, and passaged every 2-3 weeks. Established tumor organoids were trypsinized and resuspended in organoid media containing 5% basement membrane extract but lacking EGF and NRG1. 20,000 cells/well were seeded onto a basement membrane extract (50%)-coated 96-well plate and treated with trastuzumab (2–20 µg/mL), pertuzumab (50 µg/mL), MYCi361 (2–4 µM), CDIBA (5–20 µM), and/or IL-27 (50–100 ng/mL). ZMYND8 sgRNA lentivirus were transduced into cells 1 day prior to drug treatment. Seven to ten days later, the organoid viability was measured with MTS assay. Organoids were photographed using a Zeiss Axio Observer Z1 fluorescence microscope.

Human tumor studies

Human deidentified HER2+ breast tumors and their adjacent normal breast tissues were obtained from surgical breast cancer pathologists Y.F. and Y.P. for IHC studies. Staining was scored with H-score and verified by Yong Wang and Y.F[8]. The clinical responses of tumors to treatments were provided by Y.F. and Y.P.. For ZMYND8 IHC studies in paired tumors, two HER2+ tumors (Cases 1 and 2) were collected from patients after the completion of 4 cycles of trastuzumab, pertuzumab, and docetaxel. The tumor in Case 3 was a recurrent metastatic brain tumor collected from the patient 3 years after completing 4 cycles of treatment with trastuzumab, pertuzumab, and docetaxel. The biopsies collected from the same patient prior to treatments were used as controls. Gene expression data were retrieved from the PAMELA trial[25], the Alliance trial (dbGaP Study Accession: phs001291.v1.p1)[55], and TCGA downloaded from the UCSC Cancer Browser[56].

Statistics

Statistical analysis was performed using GraphPad Prism (Version 10.4.1) by 2-tailed Student's *t*-test between 2 groups, and 1- or 2-way ANOVA with multiple testing correction within multiple groups. Kaplan–Meier survival curve was analyzed by log-rank test. The number of biological replicates is shown in figures or figure legends. Each biological replicate in in vitro cell experiments includes two-three technical replicates. Data are expressed as mean ± SEM. A $p < 0.05$ was considered significant.

Data availability

The RNA-seq data were deposited at the Gene Expression Omnibus with accession number GSE245486. Gene expression data were retrieved from the PAMELA trial (NCT01973660, https://www.clinicaltrials.gov/study/NCT01973660)[25], the Alliance trial (dbGaP Study Accession: phs001291.v1.p1, https://www.ncbi.nlm.nih.gov/projects/gap/cgi-bin/study.cgi?study_id=phs001291.v1.p1)[55], and TCGA downloaded from the UCSC Cancer Browser (https://xena.ucsc.edu/welcome-to-ucsc-xena/)[56]. Source data are provided with this paper. All remaining data can be found in the Article, Supplementary and Source Data files. Source data are provided with this paper.

References

1. Meric-Bernstam, F. et al. Advances in HER2-targeted therapy: novel agents and opportunities beyond breast and gastric cancer. *Clin. Cancer Res.* **25**, 2033–2041 (2019).
2. Sawyers, C. L. Herceptin: a first assault on oncogenes that launched a revolution. *Cell* **179**, 8–12 (2019).
3. Vu, T. & Claret, F. X. Trastuzumab: updated mechanisms of action and resistance in breast cancer. *Front. Oncol.* **2**, 62 (2012).
4. Patel, T. A. et al. Dual HER2 blockade: preclinical and clinical data. *Breast Cancer Res.* **16**, 419 (2014).
5. von Minckwitz, G. et al. Adjuvant pertuzumab and trastuzumab in early HER2-positive breast cancer. *N. Engl. J. Med.* **377**, 122–131 (2017).
6. Gianni, L. et al. Efficacy and safety of neoadjuvant pertuzumab and trastuzumab in women with locally advanced, inflammatory, or early HER2-positive breast cancer (NeoSphere): a randomised multicentre, open-label, phase 2 trial. *Lancet Oncol.* **13**, 25–32 (2012).
7. Vernieri, C. et al. Resistance mechanisms to anti-HER2 therapies in HER2-positive breast cancer: Current knowledge, new research directions and therapeutic perspectives. *Crit. Rev. Oncol. Hematol.* **139**, 53–66 (2019).
8. Chen, Y. et al. ZMYND8 acetylation mediates HIF-dependent breast cancer progression and metastasis. *J. Clin. Invest.* **128**, 1937–1955 (2018).
9. Pan, Q. et al. The ZMYND8-regulated mevalonate pathway endows YAP-high intestinal cancer with metabolic vulnerability. *Mol. Cell* **81**, 2736–2751.e2738 (2021).
10. Tang, B. et al. ZMYND8 preferentially binds phosphorylated EZH2 to promote a PRC2-dependent to -independent function switch in hypoxia-inducible factor-activated cancer. *Proc. Natl Acad. Sci. USA* **118**, e2019052118 (2021).
11. Dou, C. et al. ZMYND8 promotes the growth and metastasis of hepatocellular carcinoma by promoting HK2-mediated glycolysis. *Pathol. Res. Pract.* **219**, 153345 (2021).
12. Carney, S. V. et al. Zinc finger mynd-type containing 8 (ZMYND8) is epigenetically regulated in mutant isocitrate dehydrogenase 1 (IDH1) glioma to promote radioresistance. *Clin. Cancer Res.* **29**, 1763–1782 (2023).
13. Wang, Y. et al. ZMYND8 expression in breast cancer cells blocks T-lymphocyte surveillance to promote tumor growth. *Cancer Res.* **81**, 174–186 (2021).

14. Luo, M. et al. ZMYND8 is a master regulator of 27-hydroxycholesterol that promotes tumorigenicity of breast cancer stem cells. *Sci. Adv.* **8**, eabn5295 (2022).
15. Shen, H. F. et al. The dual function of KDM5C in both gene transcriptional activation and repression promotes breast cancer cell growth and tumorigenesis. *Adv. Sci. (Weinh)* **8**, 2004635 (2021).
16. Gong, F. et al. Screen identifies bromodomain protein ZMYND8 in chromatin recognition of transcription-associated DNA damage that promotes homologous recombination. *Genes Dev.* **29**, 197–211 (2015).
17. Luo, M. et al. ZMYND8 protects breast cancer stem cells against oxidative stress and ferroptosis through activation of NRF2. *J. Clin. Invest.* **134**, e171166 (2024).
18. Perez-Pena, J. et al. Mapping Bromodomains in breast cancer and association with clinical outcome. *Sci. Rep.* **9**, 5734 (2019).
19. Dang C. V. MYC, metabolism, cell growth, and tumorigenesis. *Cold Spring Harb Perspect Med.* **3**, a014217 (2013).
20. Eiriksson, F. F. et al. Lipidomic study of cell lines reveals differences between breast cancer subtypes. *PLoS ONE* **15**, e0231289 (2020).
21. Kita, Y., Shindou, H. & Shimizu, T. Cytosolic phospholipase A(2) and lysophospholipid acyltransferases. *Biochim. Biophys. Acta Mol. Cell Biol. Lipids* **1864**, 838–845 (2019).
22. Leslie, C. C. Cytosolic phospholipase A(2): physiological function and role in disease. *J. Lipid Res.* **56**, 1386–1402 (2015).
23. Chen, L. et al. cPLA2alpha mediates TGF-beta-induced epithelial-mesenchymal transition in breast cancer through PI3k/Akt signaling. *Cell Death Dis.* **8**, e2728 (2017).
24. Ritter, C. A. et al. Human breast cancer cells selected for resistance to trastuzumab in vivo overexpress epidermal growth factor receptor and ErbB ligands and remain dependent on the ErbB receptor network. *Clin. Cancer Res.* **13**, 4909–4919 (2007).
25. Llombart-Cussac, A. et al. HER2-enriched subtype as a predictor of pathological complete response following trastuzumab and lapatinib without chemotherapy in early-stage HER2-positive breast cancer (PAMELA): an open-label, single-group, multicentre, phase 2 trial. *Lancet Oncol.* **18**, 545–554 (2017).
26. Delmore, J. E. et al. BET bromodomain inhibition as a therapeutic strategy to target c-Myc. *Cell* **146**, 904–917 (2011).
27. Gogas, H. et al. MYC copy gain, chromosomal instability and PI3K activation as potential markers of unfavourable outcome in trastuzumab-treated patients with metastatic breast cancer. *J. Transl. Med.* **14**, 136 (2016).
28. Perez, E. A. et al. C-MYC alterations and association with patient outcome in early-stage HER2-positive breast cancer from the north central cancer treatment group N9831 adjuvant trastuzumab trial. *J. Clin. Oncol.* **29**, 651–659 (2011).
29. Dueck, A. C. et al. Impact of c-MYC protein expression on outcome of patients with early-stage HER2+ breast cancer treated with adjuvant trastuzumab NCCTG (alliance) N9831. *Clin. Cancer Res.* **19**, 5798–5807 (2013).
30. Duan, N. et al. Unveiling alterations of epigenetic modifications and chromatin architecture leading to lipid metabolic reprogramming during the evolutionary trastuzumab adaptation of HER2-positive breast cancer. *Adv Sci (Weinh)* **11**, e2309424 (2024).
31. Cortese K. et al. Lipid metabolism reprogramming and trastuzumab resistance in breast cancer cell lines overexpressing the ERBB2 membrane receptor. *Membranes (Basel)* **13**, 540 (2023).
32. Donati, G. & Amati, B. MYC and therapy resistance in cancer: risks and opportunities. *Mol. Oncol.* **16**, 3828–3854 (2022).
33. Carrasco, S. & Merida, I. Diacylglycerol, when simplicity becomes complex. *Trends Biochem. Sci.* **32**, 27–36 (2007).
34. Exton, J. H. Phosphatidylcholine breakdown and signal transduction. *Biochim. Biophys. Acta* **1212**, 26–42 (1994).
35. Zuber, J. et al. RNAi screen identifies Brd4 as a therapeutic target in acute myeloid leukaemia. *Nature* **478**, 524–528 (2011).
36. Kumar-Sinha, C., Ignatoski, K. W., Lippman, M. E., Ethier, S. P. & Chinnaiyan, A. M. Transcriptome analysis of HER2 reveals a molecular connection to fatty acid synthesis. *Cancer Res.* **63**, 132–139 (2003).
37. Hanel, A. M. & Gelb, M. H. Multiple enzymatic activities of the human cytosolic 85-kDa phospholipase A2: hydrolytic reactions and acyl transfer to glycerol. *Biochemistry* **34**, 7807–7818 (1995).
38. Caiazza, F., Harvey, B. J. & Thomas, W. Cytosolic phospholipase A2 activation correlates with HER2 overexpression and mediates estrogen-dependent breast cancer cell growth. *Mol. Endocrinol.* **24**, 953–968 (2010).
39. Koundouros, N. et al. Metabolic fingerprinting links oncogenic PIK3CA with enhanced arachidonic acid-derived eicosanoids. *Cell* **181**, 1596–1611.e1527 (2020).
40. Jeong, W. C. et al. Cytoplasmic phospholipase A2 metabolites play a critical role in pulmonary tumor metastasis in mice. *Anticancer Res.* **30**, 3421–3427 (2010).
41. Mondal, S. et al. Mass spectrometry imaging of lumpectomy specimens deciphers diacylglycerols as potent biomarkers for the diagnosis of breast cancer. *Anal Chem* **95**, 8054–8062 (2023).
42. Cooke, M. & Kazanietz, M. G. Overarching roles of diacylglycerol signaling in cancer development and antitumor immunity. *Sci. Signal* **15**, eabo0264 (2022).
43. Lim, P. S., Sutton, C. R. & Rao, S. Protein kinase C in the immune system: from signalling to chromatin regulation. *Immunology* **146**, 508–522 (2015).
44. Pflanz, S. et al. IL-27, a heterodimeric cytokine composed of EBI3 and p28 protein, induces proliferation of naive CD4 + T cells. *Immunity* **16**, 779–790 (2002).
45. Isakov, N. & Altman, A. Protein kinase C(theta) in T cell activation. *Annu. Rev. Immunol.* **20**, 761–794 (2002).
46. Johnson, J. et al. A conventional protein kinase C inhibitor targeting IRF-3-dependent genes differentially regulates IL-12 family members. *Mol. Immunol.* **48**, 1484–1493 (2011).
47. Galvez, A. S. et al. Protein kinase Czeta represses the interleukin-6 promoter and impairs tumorigenesis in vivo. *Mol. Cell Biol.* **29**, 104–115 (2009).
48. Scerri, J. et al. PKC-mediated phosphorylation and activation of the MEK/ERK pathway as a mechanism of acquired trastuzumab resistance in HER2-positive breast cancer. *Front Endocrinol. (Lausanne)* **13**, 1010092 (2022).
49. Jaime-Ramirez, A. C. et al. IL-12 enhances the antitumor actions of trastuzumab via NK cell IFN-gamma production. *J. Immunol.* **186**, 3401–3409 (2011).
50. Korkaya, H. et al. Activation of an IL6 inflammatory loop mediates trastuzumab resistance in HER2+ breast cancer by expanding the cancer stem cell population. *Mol. Cell* **47**, 570–584 (2012).
51. Beizavi, Z., Zohouri, M., Asadipour, M. & Ghaderi, A. IL-27, a pleiotropic cytokine for fine-tuning the immune response in cancer. *Int. Rev. Immunol.* **40**, 319–329 (2021).
52. Griguolo, G., Pascual, T., Dieci, M. V., Guarneri, V. & Prat, A. Interaction of host immunity with HER2-targeted treatment and tumor heterogeneity in HER2-positive breast cancer. *J. Immunother. Cancer* **7**, 90 (2019).
53. Matyash, V., Liebisch, G., Kurzchalia, T. V., Shevchenko, A. & Schwudke, D. Lipid extraction by methyl-tert-butyl ether for high-throughput lipidomics. *J. Lipid Res.* **49**, 1137–1146 (2008).
54. Tang, D. et al. SRplot: A free online platform for data visualization and graphing. *PLoS ONE* **18**, e0294236 (2023).
55. Lesurf, R. et al. Genomic characterization of HER2-positive breast cancer and response to neoadjuvant trastuzumab and chemotherapy-results from the ACOSOG Z1041 (Alliance) trial. *Ann. Oncol.* **28**, 1070–1077 (2017).
56. Goldman, M. J. et al. Visualizing and interpreting cancer genomics data via the Xena platform. *Nat. Biotechnol.* **38**, 675–678 (2020).

Acknowledgements
We thank the CRI metabolomics facility for metabolite analysis, the next generation sequencing core for sequencing, and the tissue management core for assistance in IHC. We also thank Michael T. Lewis and Lacey E. Dobrolecki from the patient-derived xenograft core at the Baylor College of Medicine for BCM-4169 PDX (supported by the CPRIT grant RP220646) and Alana L. Welm at the University of Utah for HCI-032 PDX. This work was supported by grants from the NIH (R01CA222393) and the CPRIT (RR140036, RP190358) to W.L.. W.L. is a CPRIT Scholar in Cancer Research.

Author contributions
W.L. and Yingfei Wang conceived the study, analyzed the data, and wrote the paper; Yong Wang performed most experiments, analyzed the data, and wrote the paper; Yanan Wang generated plasmids; L.B. performed mouse breeding; G.V. and J.G.M. performed lipidomics analysis; Y.F. and Y.P. provided human tumor tissues; W.L., A.K. and C.X. performed bioinformatics analysis of RNAseq; F.B-M. and A.P. provided gene expression data from the PAMELA trial; C.L.A. provided isogenic BT474T/HR6, 5637/5637NR, and OVCAR8/OVCAR8NR cell lines. All authors read, edited, and approved the manuscript.

Competing interests
Yong Wang, Yingfei Wang, and W.L. are inventors on provisional patent application US 63/676,270. F.B.-M. has filed patents, including PCT/EP2022/086493, PCT/EP2023/060810, EP23382703 and EP23383369. The other authors declare no competing interests.

Additional information
Supplementary information The online version contains supplementary material available at https://doi.org/10.1038/s41467-025-59184-5.

Correspondence and requests for materials should be addressed to Weibo Luo.

Peer review information *Nature Communications* thanks Eneda Toska and the other, anonymous, reviewer(s) for their contribution to the peer review of this work. A peer review file is available.